Supporting Information

Woda et al.

SI History of Gas Development in Sugar Run area

Additional Background. Summarizing the entire history of gas well development in the Sugar Run area is beyond the scope of this contribution. We therefore emphasize the gas well closest to our study area (Table S1). This condensed summary derives from information online (1–3). Well API #081-20292 was hydraulically fractured between June 28th, 2011 and July 1st, 2011. On January 9th, 2012 the PA DEP was notified of discolored water in a private water well nearby, and since that complaint, the PA DEP determined that at least five private water supplies were impacted (1). During testing in January and February 2012, a shut-in pressure of 325 psi was measured between casing strings in the cemented annulus of 081-20292. Since April 13th, 2015, PA DEP investigated complaints of stray gas as far as 9,850 feet (3,000 meters) from the gas well and 5,200 feet (1,600 meters) from the originally affected water supplies. In June, 2015 PA DEP levied a multi-million dollar fine against the drilling company but it was rescinded in May, 2015.

SI Materials and Methods

Water Studies. ***Field measurements.*** In general in the Sugar Run area, stream flows are highest in late fall and spring after snow melt, and lowest in the summer during the hottest and driest months when evapotranspiration is highest. Multiple measurements of stream base flow were completed between SR 1 and SR 2 on Sugar Run in 5/21/2013 to 11/12/2013 (4). Discharge measured at SR 1 varied from 0.105 m^3/s in May to 0.037 m^3/s in June. During this study, sites in Sugar Run were sampled intermittently for a year and a half and at increased frequency during summer (e.g., Fig. S1). When possible, temperature, pressure, dissolved oxygen (DO), specific conductivity (SPC), pH, and oxidation and reduction potential (ORP) were measured in the field using a YSI Professional Plus meter. The YSI was calibrated before each trip using pH 4 and 7 buffers, Zobel's solution, and atmospheric oxygen. Hydrogen sulfide was measured using a Hach Hydrogen Sulfide Test Kit (Model HS-WR) in accordance with Hach protocol for a few samples.

For dissolved methane and ethane in surface waters, samples were collected using VWR polycarbonate bottles. We observed these bottles showed a memory effect for samples with high concentrations (>5 mg/L); therefore, VWR bottles containing dissolved methane >0.5 mg/L were discarded after use. The stream was sampled in the middle and approached from downstream to prevent contamination from disturbing the riverbed. Bottles were opened underwater and rinsed three times before filling and capping underwater (when water depth made this possible). If bubbles were present, the bottle was emptied and refilled. Samples for methane and ethane analyses were stored in coolers, returned to the laboratory, and prepared the night of their return for analysis (see below). Biocides were not used in any sample of groundwater or surface water collected using VWR bottles, based on tests on surface water and groundwater that showed that biocide had no effect on methane concentrations in waters in capped bottles without head space as long as the time between sampling and analysis was kept less than 5 days and, for seeps, ORP was

www.pnas.org/cgi/doi/10.1073/pnas.1809013115

relatively low. Hydrocarbon concentrations were always measured within two days of collection, and most within one day.

Over about one year, groundwater samples were collected by the authors from four homeowner wells within 1000 meters of the seep locations in Sugar Run. In every case, wells were purged for at least 15 minutes, making sure that pH and water temperature were steady for at least 5 minutes before sampling. Several authors have documented that the reproducibility of high-methane concentrations in effervescing groundwater samples is low, and much of this lack of reproducibility may be related to sampling techniques (5–8). Therefore, several sampling methods were tried for comparison and reproducibility among methods was indeed sometimes observed to be low (data from two sampling methods summarized in Dataset S1). Most samples were taken with the "inverted bottle" method (slightly modified from published procedures in that we used VWR polycarbonate bottles without biocide as described above (6)). In addition, a few samples were collected from two homeowner water wells using an Isoflask® in accordance with Isotech protocol (9). Although this collection method is now suggested to be the best method for effervescing samples (6), it was only introduced relatively recently and therefore is not as useful in comparisons with samples collected years ago. In the early years, the inverted bottle method was commonly used (e.g., (10)). We therefore emphasize samples taken with inverted bottles in discussion in main text. Hydrogen sulfide was measured using a Hach Hydrogen Sulfide Test Kit (Model HS-WR) in accordance with Hach protocol for a few samples.

Occasionally at surface and at all groundwater sites, additional samples of water were taken and then filtered with a 0.45-micron pore-size filter to be analyzed for anions and cations. Cation samples were acidified with nitric acid in the field. Samples were collected in the same way at select sites (HO4, Seep 1.5, Seep 1.6) for strontium isotope analysis. All samples were returned to the laboratory and refrigerated within 8 hours of collection.

Atmospheric methane was analyzed in the field on occasion using a Bascom-Turner Gas Rover (Fig. S3). Measurements, logged every 1-3 seconds, included location (latitude/longitude) and methane concentration in ppm (parts per million by volume). This device was calibrated using a 2.5% methane gas standard from Bascom-Turner and their internal autocalibration program.

Laboratory analyses. Cations were measured using a Perkin-Elmer Optima 5300 inductively coupled plasma atomic emission spectrophotometer (ICP-AES). Select samples were also measured using a Thermo Fisher Scientific X Series 2 Inductively Coupled Plasma Mass Spectrometer (ICP-MS) with Collision Cell Technology (Dataset S1). When the same sample was analyzed by both instruments, ICP-MS results were compared to the ICP-AES results for Fe, Al, Ba, Mn, and Sr. If concentrations were less than 0.1 mg/L and discrepant by more than 10%, ICP-MS values were reported because of their higher accuracy for low concentrations (Dataset S1). Arsenic and uranium were only measured using ICP-MS. Anion samples were analyzed using a Dionex ICS 2500 ion chromatograph (IC). Strontium isotopes ($^{87}Sr/^{86}Sr$) were measured on a Thermo Scientific Triton Plus Series Multicollector Thermal Ionization Mass Spectrometer (TIMS). Prior to analysis, strontium was purified from water samples using the Elemental Scientific prepFAST-MC automated chromatography system. The values of $^{87}Sr/^{86}Sr$ for standards run at the time of analysis were as follows: NIST SRM987 = 0.710257, BCR-1 = 0.705027, and IAPSO = 0.709194.

Hydrocarbon samples were analyzed using previously published methods at Pennsylvania State University unless otherwise noted (11, 12). First, a helium headspace was introduced to each bottle (13). These bottles were then placed on a shaker for at least 12 hours to allow dissolved gases to equilibrate with headspace. Hydrocarbons were then analyzed using a HP 5890 Series II Gas Chromatograph with a flame ionization detector and custom vacuum inlet system. $\delta\ ^{13}C\text{-}CH_4$ values were analyzed on some samples within seven days of concentration measurements according to methods outlined in previous research (12).

Noble gas sampling and analytical methods. For noble gas analyses, five water samples were collected from two domestic water wells (two duplicates from each well) in the Sugar Run area and one natural spring in Salt Spring State Park in Bradford County, PA (July 2017). These were analyzed for concentrations and isotopic ratios of the complete suite of stable noble gases (He, Ne, Ar, Kr, and Xe). Two gas samples were also collected, one from the salt spring site, the other from a seep adjacent to the Sugar Run stream (Seep 1.55) in July 2017. These two sites were chosen for gas analysis based on their high rate of bubbling. Both gas samples were analyzed for noble gas volume fractions and isotopic ratios.

For noble gas samples, groundwater was flushed through standard refrigeration grade 3/8" copper (Cu) tubes for approximately 10 min. Once temperature, pH and specific conductivity reached constant values in the outflow, Cu tubes were sealed by steel pinch-off clamps (14, 15). Additional details on groundwater sampling for noble gas analysis can be found elsewhere (16, 17). In the salt spring, a peristaltic pump was used to pump the water through the Cu tube.

To collect gas samples from the salt spring and the stream seep, a customized funnel was assembled with plastic tubes and a copper tube as shown in Figure S15 and then pre-filled with water prior to moving the funnel over the gas outlet. The funnel was kept under water continuously during sampling to allow the gas to flow through the Cu tube and to displace the water. Between 15-30 minutes were required for the Cu tube to be entirely filled with gas. The plastic tube was checked for residual water prior to closing the clamps at both ends of the copper tube.

Noble gas measurements of all water and gas samples were carried out in the Noble Gas Laboratory at the University of Michigan. He and Ne were analyzed in a Thermo Scientific Helix SFT mass spectrometer while Ar, Kr, and Xe were sequentially allowed into an ARGUS VI mass spectrometer using a computer-controlled double-head cryo-separator. Extraction, purification, and analysis procedures are described elsewhere (15, 18).

Methods for Development of Maps. ***Groundwater data and violations map.*** Several sets of groundwater data were compiled, mapped, or compared to new analyses. Most of these data were considered to represent background groundwater in the area. The largest dataset is referred to here as "pre-drill data" because it includes analytical data from commercial laboratories of samples collected by consultants for oil and gas companies (19). The companies sample groundwater within a certain distance of planned well drilling and give the data to the PA DEP to safeguard against future liability. Discussions of strengths and limitations of these types of datasets are discussed below and have been summarized elsewhere (10, 19, 20). These data were shared with the authors by the PA DEP and are published in the Shale Network database (21). In addition to this pre-drill dataset, data were summarized from other published groundwater analyses from the

Lycoming county area (22) and this entire dataset is referred to throughout as the Lycoming groundwater dataset.

In addition, available data from within the Sugar Run study area from the PA DEP were recovered using the PA DEP eMap tool (23). Another set of data – for sites in PA referred to throughout as "presumably contaminated" -- were also summarized for waters that were presumed by various government agencies to have been contaminated by oil and gas development activity (3, 24). For example, data from the US Environmental Protection Agency (US EPA) were summarized here for groundwater from water wells that were presumed to be affected by nearby shale-gas development activity (24) based on comparisons of pre-drill to post-drill hydrocarbon concentrations, hydrocarbon ratios, isotopic compositions, metal concentrations, and water type. One of these presumably impacted water wells was sampled near the alleged gas migration incident in Dimock, Pennsylvania. Six other presumably impacted water wells were sampled near an alleged gas migration event along Paradise Road in Bradford County that has also been described elsewhere (25). The final three presumably impacted water wells (GW 06, GW 01, GW 02) were reported for two other alleged gas migration incidents (24). The locations for these presumably contaminated sites were not revealed in the EPA report but locations were verified from Figures 3, 4, 33, 34, 35, and 37 of the report (24).

For these data (pre-drill or presumably contaminated samples), the commercial or government laboratories that were used for analyses are not always mentioned; however, commercial laboratories that were named include ALS Environmental, Environmental Service Laboratories, Benchmark Analytics, ESL, Fairway, Geochemical Testing, Groundwater and Environmental Services, Inc, Hess and Fisher, Lancaster, Seewald Laboratories, and Test America. The pre-drill data were originally provided by commercial analytical laboratories as paper copies or pdfs, and were transcribed into spreadsheets either by U.S. Geological Survey workers or Pennsylvania State University workers.

Data used to create Figure 1B were gathered on 8/15/2017 with the Pennsylvania Shale Viewer tool (26) and Oil and Gas Mapping Tool (27). Wells with violations were first identified using the Shale Viewer Tool. If a casing-related violation was identified, the violation was confirmed using the PA DEP Oil and Gas Mapping Tool. No discrepancies between the two tools were observed. Violations binned as casing- or cementing-related were based on guidelines outlined in previous research (28) (see also Table S1). A few additional casing-related violations were included that were not identified in the previous paper (28): 78.81(a) (Casing and Cementing - Operator conducted casing and cementing activities that failed to prevent migration of gas or other fluids into sources of fresh groundwater); 78.81(a)3 (Casing and Cementing - Operator conducted casing and cementing activities that failed to prevent pollution or diminution of fresh groundwater); OGA 3217(B) (Failure to prevent migration of gas or fluids into sources of fresh water causing pollution or diminution, failure to properly case and cement well through a fresh water-bearing strata in regulated manner or depth).

Construction of structural geology model. A three-dimensional model was constructed for the eastern end of the Nittany Anticlinorium based on well and map data (Fig. S5). Well data consisted of formation logs from 22 gas wells in the area (2). These mostly include the Marcellus and units stratigraphically above it, although a few extend deeper (29–31). Data were digitized and analyzed with Midland Valley's Move™ software. Cross sections derived from two datasets (29, 30) were also digitized and added to the model. These sections were extended and additional sections were

created based on map and well data to represent the three-dimensional structure of the anticline more completely. The cross sections and the well data were then used to create three-dimensional surfaces by ordinary kriging.

A block diagram (Fig. S5) and a cross section (Fig. 1D) from the closest gas well 081-20292 to Sugar Run were created from the surfaces. The block diagram was slightly edited manually in areas where the kriging was poorly constrained by data in order to remove geologically unrealistic artifacts or to smooth horizons. The surface representing the top of the Marcellus Formation was contoured to produce a structural contour map of this horizon (Fig. S13).

SI Results and Discussion

Field Measurements. The pH of seeps (5.9 to 7.0) was lower than observed in Sugar Run (7.1 to 8.2) which was generally lower than observed in nearby homeowner water wells (7.6 to 8.9). In contrast, oxidation reduction potential (ORP) decreased from the stream (177 to 241 mV) to the seeps (-90 to 169 mV) to the homeowners' water wells (-277 to -146 mV). Late in our investigation we discovered another seep that had the highest pH (9.1) of any samples and had dark black sediment. This bubbling seep (SRS 1.5, Fig. 1) was in a channel of a small intermittent tributary where we had limited permission for sampling.

Comparison of Groundwater Hydrocarbon Samples. As discussed in SI Materials and Methods, the groundwater samples we report in Figure 2 were limited to those collected with the inverted bottle technique so as to compare concentrations over a longer period of time for samples collected in the same manner.

Three (HO2, HO3, HO4) out of the four homeowner water wells that we sampled in this study were observed to effervesce. As discussed in SI Materials and Methods, large variability was observed in these high-methane samples for methane concentrations (concentrations were generally >20 mg/L) when collected with different methods (two are summarized in Dataset S1). For example, samples collected from HO2 and HO4 using the Isoflask® method contained CH_4 concentrations of 28.0 mg/L and 49.0 mg/L, respectively. In comparison, methane concentrations of HO2 and HO4 water samples collected at the same time using the inverted bottle method were analyzed to contain 26.4 mg/L and 29.1 mg/L respectively (Dataset S1). Groundwater at both HO2 and HO4 were observed to effervesce.

Ethane concentrations for samples collected using the inverted bottle method (594 µg/L) and using the Isoflask® (1,200 µg/L) were also observed to differ for water well HO4. Propane was detected in one Isoflask sample (HO4) by Isotech laboratories (Dataset S1).

Noble Gas Data. ***Noble gas data overview.*** Noble gas concentrations (for water samples), volume fractions (for gas samples), and isotopic ratios (for both water and gas samples) are listed in Table S2-S4, respectively. Dissolved methane concentrations of water samples are also included in Table S2. Measured $^3He/^4He$ (R) ratios of water and gas samples are normalized to the corresponding atmospheric value ($Ra = 1.384 \times 10^{-6}$) and shown as R/Ra in Table S4. R/Ra values of all gas samples and the salt spring water sample are particularly low (0.0114 ± 0.0005 to 0.0165 ± 0.0006),

pointing to the presence of a highly pristine crustal signature while well water samples are higher and fall within the range of typical crustal *R/Ra* ratios (~0.02-0.05) (32). These *R/Ra* values are much lower than the atmospheric value (*R/Ra* = 1), strongly suggesting the presence of a largely dominant contribution of crustal helium. This also shows that our sampling technique successfully preserves pristine noble gas signatures. Isotopic ratios of all other gases are atmospheric within a 2σ error with only a few exceptions (e.g., $^{40}Ar/^{36}Ar$ values of HO4). For example, the isotopic ratios for Ne, Kr, and Xe are mostly consistent with atmospheric origin. These gases are incorporated into the subsurface by recharge water in equilibrium with the atmosphere (i.e., air-saturated water or ASW). Figure S16 shows $^{4}He/^{36}Ar$, $^{22}Ne/^{36}Ar$, $^{84}Kr/^{36}Ar$, and $^{132}Xe/^{36}Ar$ ratios normalized to corresponding air values and plotted as *F(i)* where *F* denotes the ratio of isotope *i* to ^{36}Ar in air. From Figure S16, it is apparent that $F(^{4}He)$ values for all samples are far higher (>1 to 3 orders of magnitude) than both air and ASW values at 10 °C, pointing to an almost entire dominance of crustal He. A temperature of 10°C for the ASW component was chosen to represent recent recharge conditions in northeastern PA.

$F(^{22}Ne)$ ratios of gas samples are higher than that of ASW while their $F(^{84}Kr)$ and $F(^{132}Xe)$ ratios are lower than corresponding ASW values. However, $F(^{22}Ne)$, $F(^{84}Kr)$, and $F(^{132}Xe)$ values of water samples generally display exactly the opposite pattern from the gas samples (except for $F(^{22}Ne)$ ratios of water samples from homeowner wells). Such patterns of noble gas elemental ratios were also observed in methane-rich groundwater within the Barnett Shale footprint and corresponding Barnett and Strawn shale gas (15, 18). Because the solubility of noble gases increases with atomic weight, light noble gases (i.e., ^{22}Ne) will preferentially partition into the gas phase when groundwater degasses. A single-stage water degassing model can therefore explain the relative depletion of light ^{22}Ne and relative enrichment of heavy ^{84}Kr and ^{132}Xe observed in salt spring water. The $F(^{22}Ne)$ values of well water samples mimic ASW values (Figure S16), suggesting limited noble gas fractionation. This might be due to a short contact time between the gas and liquid phases.

Source of helium and methane: shallower vs. deeper formations. As shown above, crustal He largely dominates the total measured He. To evaluate whether crustal He is produced in-situ in the shallower formations (i.e., Upper Devonian strata such as the Lock Haven Formation) (4) or has an external origin (i.e., deeper formations such as the Marcellus Formation), ^{4}He ages were calculated for all water samples assuming that all crustal ^{4}He is produced within the Lock Haven Formation as follows:

$$A_{^{i}He} = P(^{i}He) \times \rho_r \times \Lambda \times ((1-\omega)/\omega) cm^3 STP g_{H2O}^{-1} yr^{-1} \quad (1)$$

$$P(^{4}He) = 1.207 \times 10^{-13}[U] + 2.867 \times 10^{-14}[Th] cm^3 STP g_{rock}^{-1} yr^{-1} \quad (2)$$

Here, ρ_r is the density of the rock in g/cm^3, ω is the porosity of the reservoir rock, Λ is the transfer efficiency of He from the rock matrix to the water (assumed to be 1), U and Th represent uranium and thorium concentrations (in mg/kg) respectively in the host rock. The rock density is assumed to be 2.5 g/cm^3 while the porosity is set to 0.2. Average U and Th contents for the Lock Haven Formation were set to 2.6 and 9.7 mg/kg, respectively, following a recent publication (33).

Calculated ^{4}He ages are listed in Table S2 and range from 0.37 Ma to 0.85 Ma. These ages are much older than the previously reported, mostly modern ages (11). These ^{4}He ages calculated here are much larger than reasonable residence times for shallow groundwater, indicating that in-

situ production is not responsible for most of the crustal ^{4}He present in this groundwater. An external source of ^{4}He must be introduced to account for the majority of measured ^{4}He concentrations in these groundwater samples. This external source might also bring thermogenic methane into the shallow aquifer as thermogenic methane contents usually correlate positively with crustal He content in groundwater (15, 33).

The presence of crustal ^{40}Ar ($^{40}Ar^{*}$) was detected in water samples collected from a homeowner well (HO4) and in a gas sample from Seep 1.55 (Table S4). Calculated $^{4}He/^{40}Ar^{*}$ ratios of sample HO4 range from 7.49 to 9.01, values within the previously reported range (6.2-13.7) of natural gas samples from the Marcellus Formation (34) but over an order of magnitude lower than reported natural gas sample values (214.6-285.4) from the Upper Devonian formations (i.e., Canadaway Formation) (34). This leads to the inference that the Marcellus Formation is likely to be the external source of both crustal noble gas and thermogenic methane in the samples of HO4. Noble gas fractionation due to water degassing, which might alter the original $^{4}He/^{40}Ar^{*}$, is not considered possible here for HO4 because the fractionation is limited for water samples collected from homeowner wells (Figure S16). However, the gas sample from Seep 1.55 displays $^{4}He/^{40}Ar^{*}$ values of 82.57-98.29, which might be consistent with some mixing of Marcellus gas and Upper Devonian gas. Alternatively, degassing of the water could preferentially have released some of the light ^{4}He into the gas phase but have retained the heavier ^{40}Ar in the water phase. This mechanism is a possible explanation for the increased $^{4}He/^{40}Ar^{*}$ observed in Seep 1.55.

Mechanism of methane migration: free gas vs. dissolved phase. Natural gas can be transported as a free gas phase or as a dissolved species in groundwater and such transport might happen naturally, perhaps along with brine salts, or as a result of hydrocarbon production activities, e.g., drilling or hydraulic fracturing (18, 25, 34–36).

To further determine how the external Marcellus gas migrates into the shallow aquifer in the Sugar Run area, we plotted $^{4}He/CH_4$ as a function of $^{20}Ne/^{36}Ar$ for well water samples (Figure S9). Predicted $^{4}He/CH_4$ and $^{20}Ne/^{36}Ar$ ratios were calculated for four scenarios (33): (1) slow upward advection of water containing brine salts and dissolved methane; (2) diffusion of gas from depth through aqueous solution; (3) combined upward advection of two phases (i.e., free gas phase and brine salt-containing water phase); and (4) fast upward advection of free phase gas with minor mixing of microbial gas in the shallow aquifer. Note, we assumed that microbial gas contributes methane but not noble gases. For all scenarios, we assumed the starting point was the composition of Marcellus production gas (green square in Figure S9). Since the chloride concentrations in water collected from HO2 and HO4 are very low (< 10 mg/L), we can exclude scenario (1). From Figure S9, $^{4}He/CH_4$ and $^{20}Ne/^{36}Ar$ ratios of water samples HO2 and HO4 are distinct from predictions for scenarios (2) and (3), and thus argue against gas migration coupled with aqueous solution as a two-phase system. In contrast, short-timescale migration of natural gas in a free gas phase (scenario (4), e.g., gas leaking from a faulty gas well that then migrates along faults and fractures) could maintain the original noble gas and hydrocarbon ratios with minimal fractionation. The difference in $^{4}He/CH_4$ and $^{20}Ne/^{36}Ar$ values between Marcellus production gas and water samples is attributed either to variability of noble gas composition of Marcellus production gas or to the input of a small amount of microbial methane (as shown and labelled along line (4)).

In summary, while other interpretations are possible – i.e., multiple sources of gas and multiple migration and oxidation steps -- these noble gas data are consistent with the interpretation that thermogenic methane detected in water wells HO2 and HO4 within the Sugar Run area is from

the Marcellus Formation. These Marcellus gases most likely migrate into the shallow aquifer in a free gas phase along faults, fractures, and porous formations.

Seasonal Changes. Seasonal changes in methane concentrations for the most methane-rich seep, Seep 1.6 (Fig. S7), were not simply caused by dilution: methane was typically most concentrated during the winter and early spring when water levels were at their highest, and smallest during the summer months when water levels were lowest. This observation argues against methane migration as a dissolved solute; seasonally high methane concentrations in the wetter months are therefore attributed largely to free-phase methane moving upward, sometimes entrained in groundwaters as they move within the shallow surface. Free-phase gas migration may also be consistent with the observations of methane emitting from fractures in outcrops near the study site (Fig. 1C). This explanation for the mechanism of migration (free-phase gas) is also consistent with noble gas data discussed above and with published arguments for the Sugar Run site (11).

The similarity in seasonal changes in methane, iron, and arsenic concentrations for Seep 1.6 are consistent with the explanation that methane concentrations drive iron and arsenic variability (Fig. S7). Specifically, we argue that iron is observed at higher concentrations at Seep 1.6 when subsurface bacteria couple methane oxidation to iron reduction. (Ferric iron minerals are much less soluble than ferrous iron minerals at circumneutral pH). It is well known that oxygen does not diffuse as easily through water-filled as compared to air-filled pores (37). Consequently, the enhanced water saturation and lower subsurface oxygen concentrations during the wet season at Sugar Run likely accelerate anaerobic oxidation of methane coupled to reduction of ferric iron oxide minerals, releasing ferrous iron to solution.

In the summer when water saturation of porous subsurface material is lower, less methane likely reaches the surface because it is not entrained as much in upflowing groundwater. In addition, oxygen is more abundant in the less water-saturated subsurface and can be used by bacteria as the electron acceptor for aerobic methane oxidation instead of ferric iron. This draws down oxygen but does not release ferrous iron to solution. According to this explanation, low methane concentrations in the summer are caused both by low upflow rates of groundwater with entrained free-phase methane in the shallow subsurface and by high rates of methane oxidation by oxygen, the thermodynamically preferred oxidant.

The release of arsenic to solution seasonally documented in Figure S7 is consistent with anaerobic methane oxidation that reduces ferric iron oxides to release iron and adsorbed arsenic into solution (38). This is especially notable because arsenic is a known carcinogen and thus could be of concern in drinking water systems (39). In Seep 1.6, concentrations above the EPA drinking water standard were never measured (Dataset S1).

Using Salt Tracers to Identify Groundwater That Warrants Further Investigation. ***Chloride concentrations*****.** In this section we explore whether concentrations of Cl, Na, and Ca could be useful tools in identifying water supplies that contain methane derived from non-natural sources. These tools may be specific to the northeastern USA where natural dissolved thermogenic methane is often detected with fluids that contain salts from Appalachian Basin brine (ABB). Specifically, in the Appalachian Basin, naturally high methane concentrations correlate with high chloride (40–42). Some have even suggested that non-impacted groundwaters with naturally high chloride concentrations in PA may document connections to deeper fracture networks that could be locations for easy gas migration if gas wells allow leakage nearby (43).

To investigate such correlations, we plotted the Lycoming groundwater dataset (21), assumed to represent natural background, with groundwaters from the Sugar Run area and from the presumably impacted water wells in Fig. S12 (3, 23, 24, 44) to see if any waters are chemically distinct. As shown in Figure S12A, almost all high-methane samples from the Lycoming groundwater dataset contained high chloride (>30 mg/L) whereas almost all the presumably impacted samples -- and Sugar Run samples -- contained very low chloride (<30 mg/L).

Figure S12A documents that samples near Sugar Run are anomalous in that they are high in methane and low in chloride. Such samples could be explained by at least two scenarios. First, methane could be produced biogenically in low chloride waters: such a mechanism can explain high methane in swamps, for example. Second, methane could migrate in a free gas phase independent of ABB-containing waters (11). This second scenario is more likely for Sugar Run waters and the presumably affected waters since many of those waters were shown to contain thermogenic methane, as determined from isotopic analysis and C1/C2 ratios (24). In addition, migration of free gas for Sugar Run was consistent with noble gas analysis (Fig. S9) and other considerations (11). Wetlands were also not observed in the bedrock-lined channel of Sugar Run.

Na-rich versus Ca-rich waters. In the Appalachian Basin, higher methane concentrations have also been associated with Na-rich as opposed to Ca-rich waters (45). Ca-rich waters are believed to represent near-surface recharge or shallow groundwater (22, 46). In this light, we hypothesized that Ca-rich high-methane waters are less likely to contain thermogenic methane from natural sources.

We tested datasets to see if such inferences would be useful in highlighting anomalous methane concentrations in groundwaters, i.e., methane that warrants further investigation because it might be related to anthropogenic activities. On a plot showing the ratio of Ca to Na concentrations for the Lycoming data and the presumably impacted waters (Figure S12B), fewer outliers are detected in the blue quadrant compared to outliers on Figure S12A. Most of the samples, regardless of the source of data, have Ca/Na <0.52. However, some samples from Sugar Run and the presumably impacted water wells have Ca/Na >0.52. This shows that relatively Ca-rich high-methane water samples are another water type that warrant further investigation to detect a recent invasion of methane gas.

References:

1. The Pennsylvania Environmental Hearing Board (2017) *Commonwealth of Pennsylvania Department of Environmental Protection vs Range Resources* Available at: http://ehb.courtapps.com/public/document_shower_pub.php?csNameID=5093 [Accessed May 1, 2018].
2. Edwin Exploration and Development Well Information Network Available at: https://edwin.onbaseonline.com/1500AppNet/Login.aspx [Accessed July 27, 2018].
3. Range Resources - Appalachia, LLC, Green Valley Rd Water Well Investigation Moreland TWP, Lycoming Co., PA (2013) Available at: http://www.rangeresources.com/docs/default-source/lycoming/range-final-report-4-8-12.pdf?sfvrsn=2 [Accessed November 7, 2017].
4. Heilweil VM, et al. (2015) Stream measurements locate thermogenic methane fluxes in groundwater discharge in an area of shale-gas development. *Environ Sci Technol*

49(7):4057–4065.
5. Rivard C, Bordeleau G, Lavoie D, Lefebvre R, Malet X (2018) Can groundwater sampling techniques used in monitoring wells influence methane concentrations and isotopes? *Environ Monit Assess* 190(4). doi:10.1007/s10661-018-6532-7.
6. Molofsky LJ, et al. (2016) Effect of different sampling methodologies on measured methane concentrations in groundwater samples. *Groundwater* 54(5):669–680.
7. Jackson RE, Heagle DJ (2016) Sampling domestic/farm wells for baseline groundwater quality and fugitive gas. *Hydrogeol J* 24(2):269–272.
8. Smith B, Becker M, Siegel D (2016) Temporal variability of methane in domestic groundwater wells, northeastern Pennsylvania. *Environ Geosci* 23(1):49–80.
9. Isotech Laboratories (2011) Collection of Ground Water Samples from Domestic and Municipal Water Wells for Dissolved Gas Analysis Using IsoFlasks. (877). Available at: http://www.isotechlabs.com/products/isoflask/ISOFLASK_SAMPLING.pdf [Accessed January 1, 2018].
10. Siegel DI, Azzolina NA, Smith BJ, Perry AE, Bothun RL (2015) Methane concentrations in water wells unrelated to proximity to existing oil and gas wells in northeastern Pennsylvania. *Environ Sci Technol* 49(7):4106–4112.
11. Grieve PL, et al. (2018) Using environmental tracers and modelling to identify natural and gas well-induced emissions of methane into streams. *Appl Geochemistry* 91:107–121.
12. Wendt AK, et al. (2018) Scientist-nonscientist teams explore methane sources in streams near oil/gas development. *J Contemp Water Res Educ* 164(1):80–111.
13. Kampbell DH, Vandegrift S a (1998) Analysis of dissolved methane, ethane, and ethylene in ground water by a standard gas chromatographic technique. *J Chromatogr Sci* 36(5):253–256.
14. Weiss RF (1968) Piggyback sampler for dissolved gas studies on sealed water samples. *Deep Res Oceanogr Abstr* 15(6):695–699.
15. Wen T, et al. (2016) Methane sources and migration mechanisms in shallow groundwaters in Parker and Hood Counties, Texas - A heavy noble gas analysis. *Environ Sci Technol* 50(21):12012–12021.
16. Castro MC, Warrier RB, Hall CM, Lohmann KC (2012) A late Pleistocene-Mid-Holocene noble gas and stable isotope climate and subglacial record in southern Michigan. *Geophys Res Lett* 39(19):1–6.
17. Wen T, Castro MC, Hall CM, Pinti DL, Lohmann KC (2015) Constraining groundwater flow in the glacial drift and Saginaw aquifers in the Michigan Basin through helium concentrations and isotopic ratios. *Geofluids* 16(1):3–25.
18. Wen T, et al. (2017) Characterizing the noble gas isotopic composition of the Barnett Shale and Strawn Group and constraining the source of stray gas in the Trinity Aquifer, north-central Texas. *Environ Sci Technol* 51(11):6533–6541.
19. Li Z, et al. (2016) Searching for anomalous methane in shallow groundwater near shale gas wells. *J Contam Hydrol* 195:23–30.
20. Wen T, et al. (2018) Big groundwater datasets reveal possible rare contamination amid otherwise improved water quality for some analytes in a region of Marcellus Shale development. *Environ Sci Technol* 52:7149–7159.
21. Brantley, S.L., 2018. Shale Network Database, Consortium for Universities for the Advancement of Hydrologic Sciences, Inc. (CUAHSI), https://doi.org/10.4211/his-data-shalenetwork.

22. Gross E, Cravotta III C (2016) Groundwater Quality for 75 Domestic Wells in Lycoming County, Pennsylvania, 2014. U.S. Geological Survey Scientific Investigations Report 2016-5143, 74 p (US Geological Survey, Reston, VA). https://doi.org/10.3133/sir20165143.
23. PA DEP eMapPA. Available at: http://www.depgis.state.pa.us/emappa/ [Accessed January 1, 2017].
24. U. S. Environmental Protection Agency. 2015. *Retrospective Case Study in Northeastern Pennsylvania: Study of the Potential Impacts of Hydraulic Fracturing on Drinking Water Resources*. Office of Research and Development EPA/600/R-14/088: www.epa.gov/hfstudy [Accessed January 1, 2017].
25. Llewellyn GT, et al. (2015) Evaluating a groundwater supply contamination incident attributed to Marcellus Shale gas development. *Proc Natl Acad Sci* 112(20):6325–6330.
26. PA Shale Viewer Available at: https://www.fractracker.org/map/us/pennsylvania/pa-shale-viewer/ [Accessed August 15, 2017].
27. PA Oil and Gas Mapping Available at: http://www.depgis.state.pa.us/PaOilAndGasMapping/OilGasWellsStrayGasMap.html? [Accessed August 15, 2017].
28. Brantley SL, et al. (2014) Water resource impacts during unconventional shale gas development: The Pennsylvania experience. *Int J Coal Geol* 126:140–156.
29. Faill, R. T. (1979). Geology and Mineral Resources of the Montoursville South and Muncy Quadrangles and Part of the Hughesville Quadrangle, Lycoming, Northumberand, and Montour Counties, Pennsylvania Atlas 144ab (Commonwealth of Pennsylvania, Department of Environmental Resources, Bureau of Topographic and Geologic Survey, Harrisburg, PA).
30. Wells, R. B., & Bucek, M. F. (1980). Geology and mineral resources of the Montoursville North and Huntersville quadrangles, Lycoming County, Pennsylvania (Pennsylvania Bureau of Topographic and Geologic Survey, Harrisburg, PA).
31. Miles, C.E., Whitfield, T.G., et al., 2001. Bedrock Geology of Pennsylvania, 4th ser., dataset, scale 1:250,000 (Pennsylvania Geological Survey, Harrisburg, PA).
32. Oxburgh E., O'Nions R., Hill R. (1986) Helium isotopes in sedimentary basins. *Nature* 324:632–635.
33. Darrah TH, et al. (2015) The evolution of Devonian hydrocarbon gases in shallow aquifers of the northern Appalachian Basin: Insights from integrating noble gas and hydrocarbon geochemistry. *Geochim Cosmochim Acta* 170:321–355.
34. Darrah TH, Vengosh A, Jackson RB, Warner NR, Poreda RJ (2014) Noble gases identify the mechanisms of fugitive gas contamination in drinking-water wells overlying the Marcellus and Barnett Shales. *Proc Natl Acad Sci* 111(39):14076–14081.
35. Li H, Carlson KH (2014) Distribution and Origin of Groundwater Methane in the Wattenberg Oil and Gas Field of Northern Colorado. *Environ Sci Technol* 48(3):1484–1491.
36. Molofsky LJ, Connor JA, Wylie AS, Wagner T, Farhat SK (2013) Evaluation of Methane Sources in Groundwater in Northeastern Pennsylvania. *GroundWater* 51(3):333–349.
37. Feng G, Wu L, Letey J (2002) Evaluating Aeration Criteria By Simultaneous Measurement of Oxygen Diffusion Rate And Soil-Water Regime. *Soil Sci* 167(8):495–503.
38. Campbell KM, Malasarn D, Saltikov CW, Newman DK, Hering JG (2006) Simultaneous microbial reduction of iron(III) and arsenic(V) in suspensions of hydrous ferric oxide. *Environ Sci Technol* 40(19):5950–5955.
39. Meliker J, Slotnick M, AvRuskin G, Schottenfeld D, Jacque (2010) Lifetime exposure to

arsenic in drinking water and bladder cancer: a population-based case–control study in Michigan, USA. *Natl Institues Heath* 21(5):745–757.
40. Harkness JS, et al. (2015) Iodide, bromide, and ammonium in hydraulic fracturing and oil and gas wastewaters: Environmental implications. *Environ Sci Technol* 49(3):1955–1963.
41. Kreuzer RL, et al. (2018) Structural and hydrogeological controls on hydrocarbon and brine migration into drinking water aquifers in southern New York. *Groundwater* 56(2):225–244.
42. Llewellyn GT (2014) Evidence and mechanisms for Appalachian Basin brine migration into shallow aquifers in NE Pennsylvania, USA. *Hydrogeol J* 22(5):1055–1066.
43. Warner NR, et al. (2012) Geochemical evidence for possible natural migration of Marcellus Formation brine to shallow aquifers in Pennsylvania. *Proc Natl Acad Sci* 109(30):11961–11966.
44. Range Resources - Appalachia, LLC, Green Valley Rd Water Well Investigation Moreland TWP, Lycoming Co., PA, (2012) Available at: http://www.rangeresources.com/docs/default-source/lycoming/appendix-iv-range-presentation-to-pa-dep-10-1-12.pdf?sfvrsn=2 [Accessed June 29, 2017].
45. Molofsky LJ, et al. (2016) Environmental Factors Associated With Natural Methane Occurrence in the Appalachian Basin. *Groundwater* 54(5):656–668.
46. Siegel DI, Smith B, Perry E, Bothun R, Hollingsworth M (2015) Pre-drilling water-quality data of groundwater prior to shale gas drilling in the Appalachian Basin: Analysis of the Chesapeake Energy Corporation dataset. *Appl Geochemistry* 63(June):37–57.
47. Whiticar MJ (1999) Carbon and hydrogen isotope systematics of bacterial formation and oxidation of methane. *Chem Geol* 161(1–3):291–314.
48. Coleman D, Risatti B, Schoell M (1981) Fractionation of carbon and hydrogen isotopes by methane-oxidizing bacteria. *Geochemica* 45:1033–1037.
49. USGS Produced Waters. Available at: https://energy.usgs.gov/EnvironmentalAspects/EnvironmentalAspectsofEnergyProductionandUse/ProducedWaters.aspx#3822349-data [Accessed January 2, 2018].
50. Ozima M, Podosek F (2002) *Noble Gas Geochemistry* (Cambridge University Press, New York).
51. PA DEP OG Compliance - Report Viewer. Pennsylvania Department of Environmental Protection Oil and Gas website. Available at: http://www.depreportingservices.state.pa.us/ReportServer/Pages/ReportViewer.aspx?/Oil_Gas/OG_Compliance [Accessed August 15, 2017].

SI Figures

Figure S1. Photograph of Sugar Run showing Seep 1.5 (left) and the stream (right).

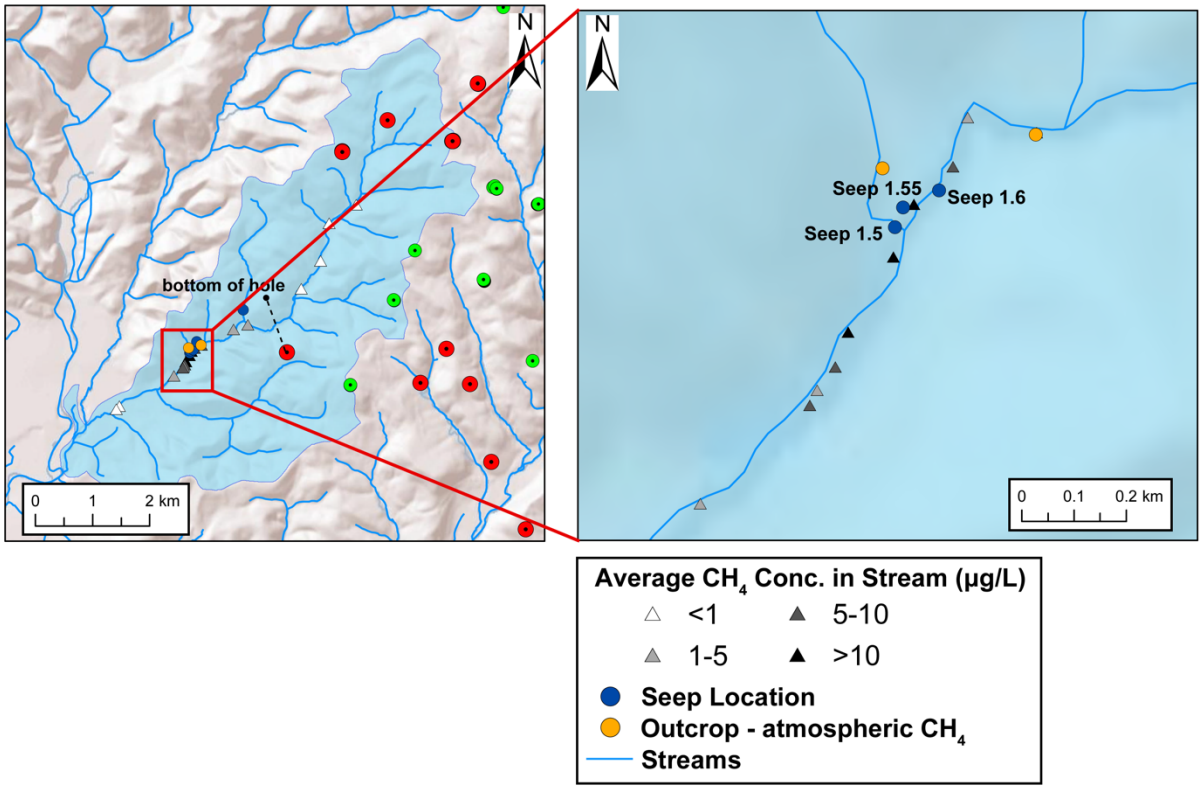

Figure S2. A) Map of the Sugar Run watershed (colored blue), sample locations (triangles), seepage locations (blue circles), and outcrops (orange circles). B) Map of Sugar Run sampling locations with seeps and the average stream methane concentrations at each site. Active bubbling was observed in the stream and seeps along this stretch. The dashed line and red and green symbols in (A) are described in caption for Figure 1.

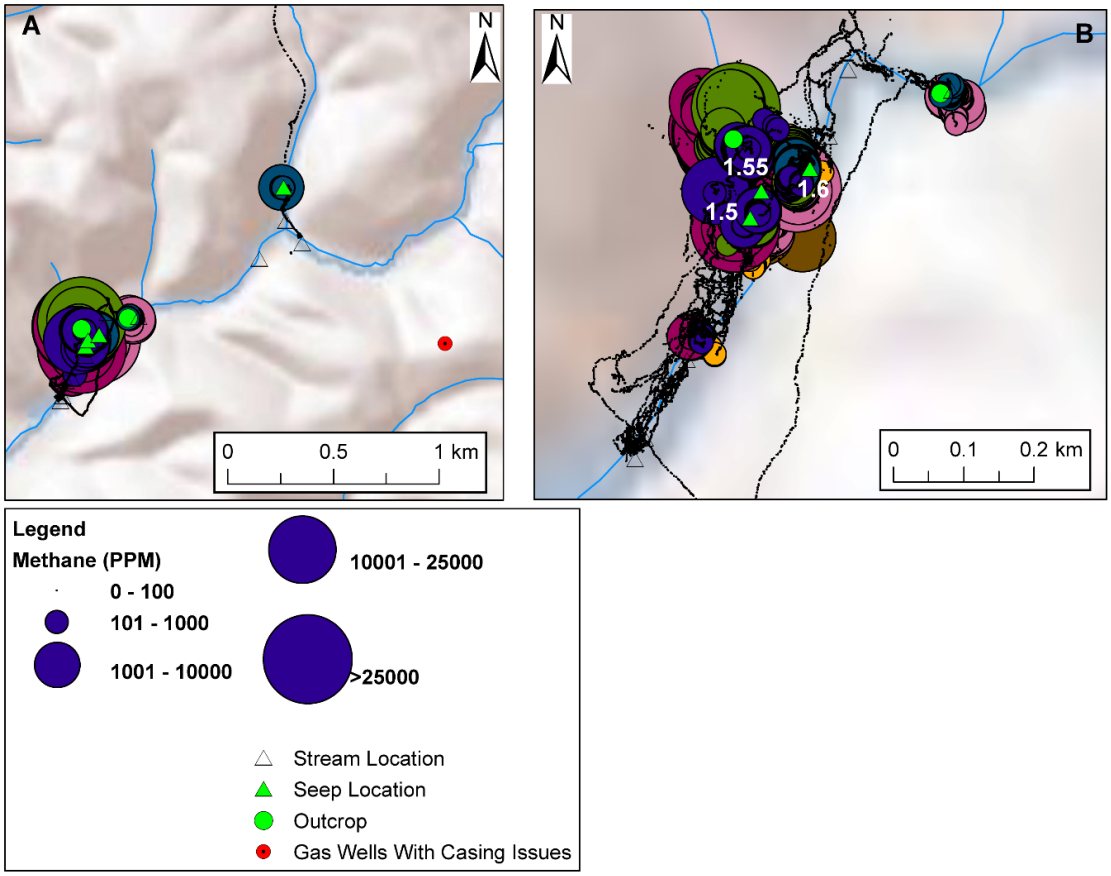

Figure S3. (A) Map showing measurements of methane concentrations in air measured on eight different days in the study region. Distinct colors represent different sampling days while the sizes of the symbols indicate concentration. (B) Methane concentration map for air in the highest-concentration region. Over 24,000 measurements were collected over 8 days. Measurements were completed by walking around the study region and holding a surface bell probe within one meter of the ground surface. At outcrops, the surface bell probe was placed directly on fractures.

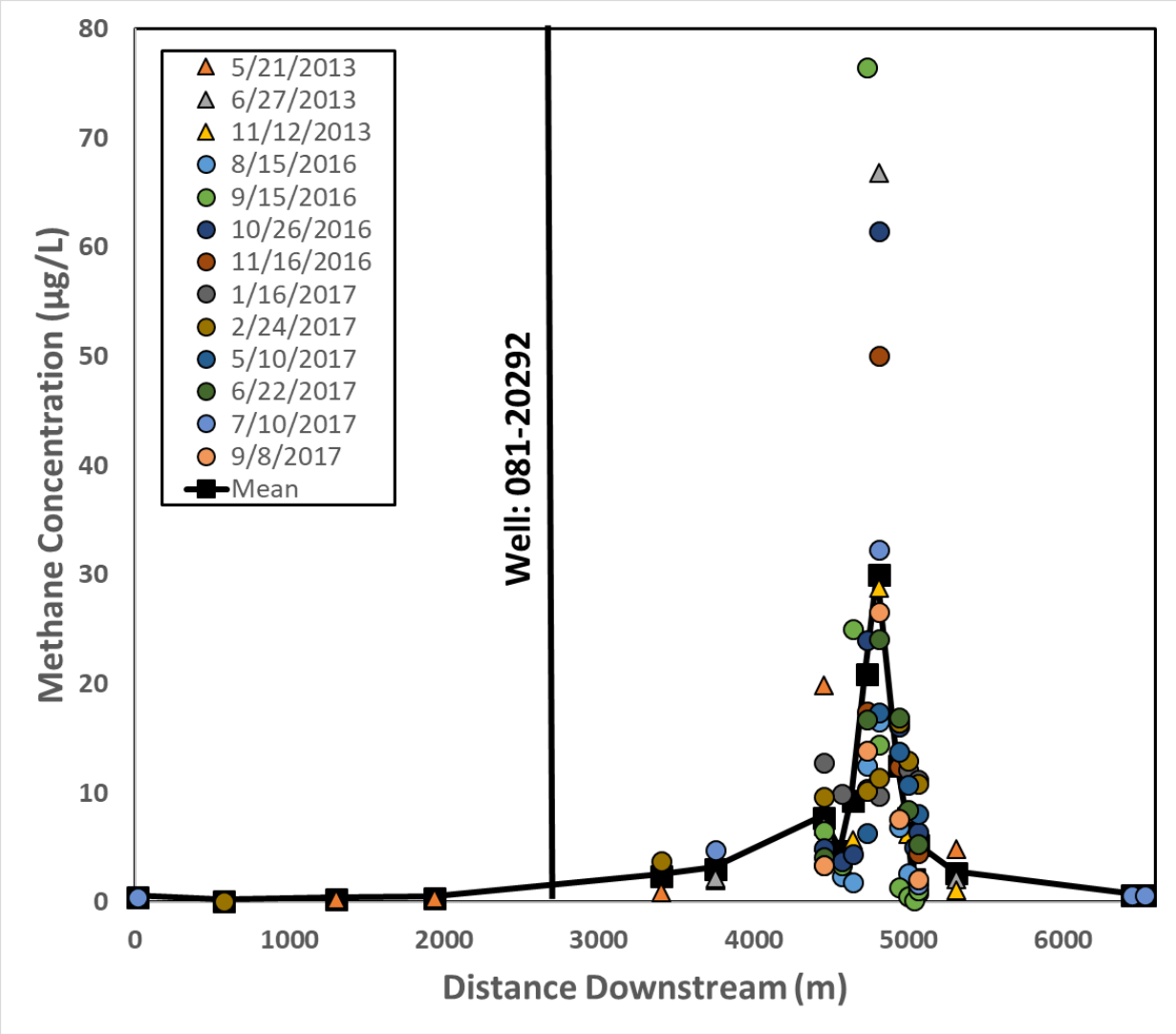

Figure S4. Methane concentration in stream water plotted versus distance downstream along Sugar Run in Lycoming County, Pennsylvania. The zero position was defined as the most upstream stream site (SR 8) that was sampled. Triangles are samples collected and analyzed by Heilweil et al. (4) and circles represent samples from this study. Largest methane concentrations in the stream consistently were measured at sites SR 1.5 and SR 1.55 (near two methane-rich seeps). The horizontal section of well 081-20292 crosses underneath Sugar Run at the line, and locations downstream of this location are structurally up dip.

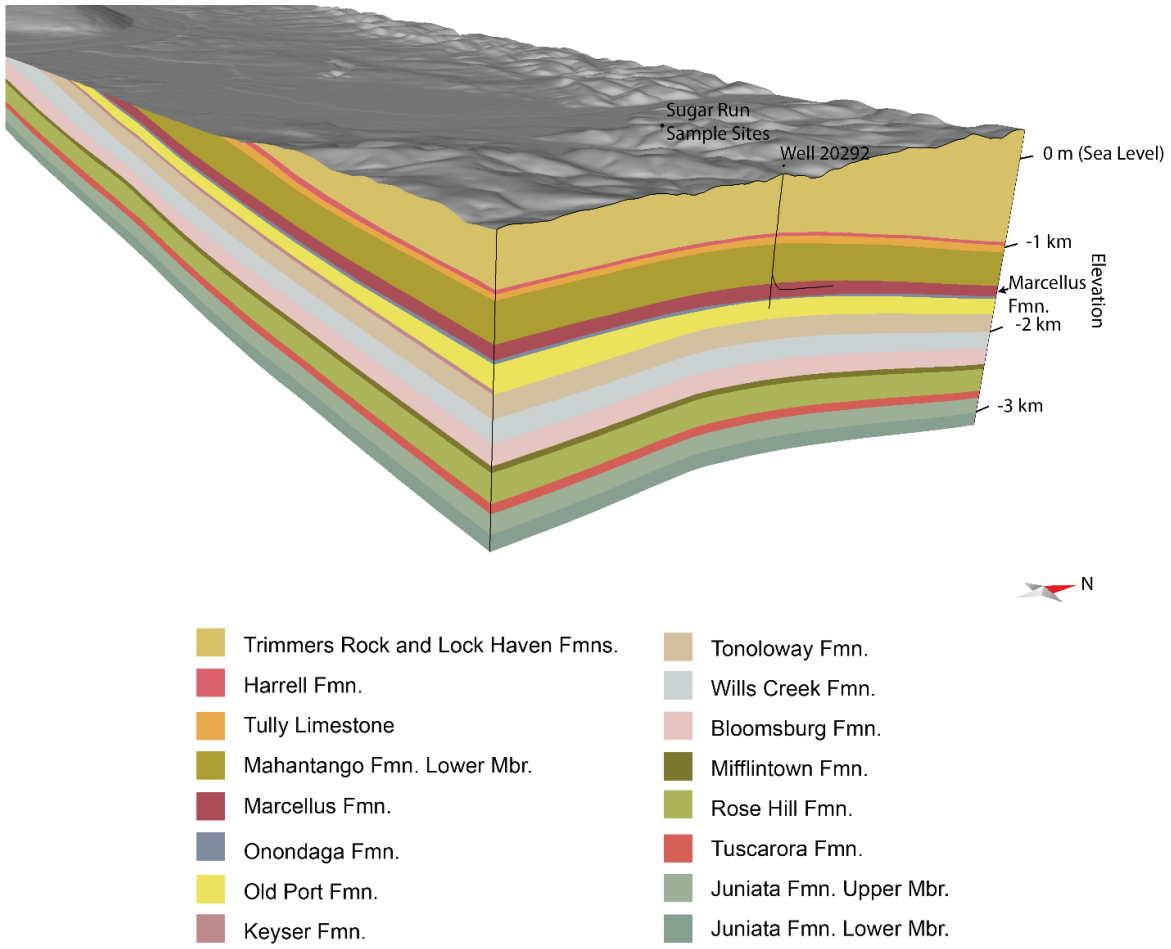

Figure S5. Block diagram of the Nittany Anticlinorium, showing locations of Sugar Run and gas well 081-20292. The surface impression of the Nittany Anticlinorium can be observed to the west in the figure.

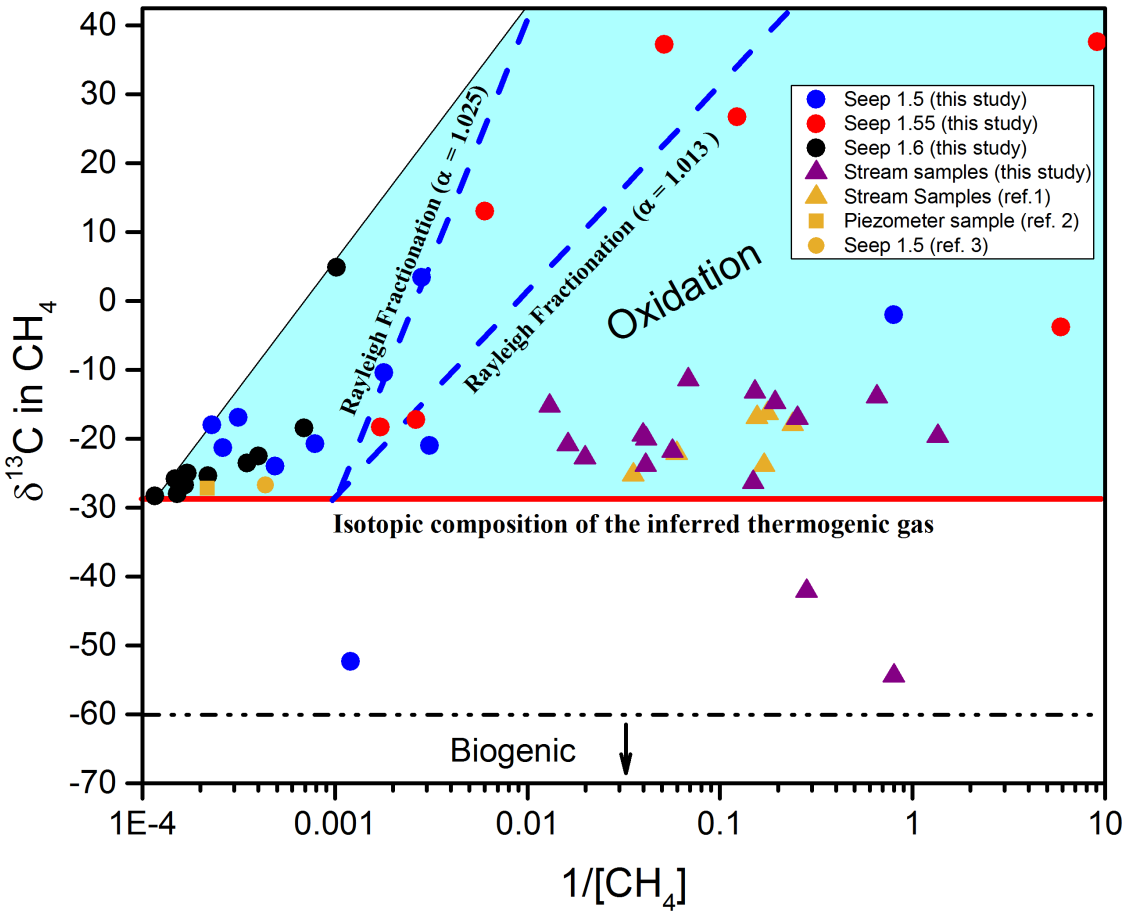

Figure S6. Isotopic values for methane from samples collected at sites in Figure S2 plotted versus 1/[CH_4] where [CH_4] refers to CH_4 concentrations in µg/L. In the blue region, $\delta^{13}C$ increases with decreasing methane concentration, as expected for fractionation during methane oxidation (47). A few samples more negative than -28.3‰ plot outside the blue area and approach an inferred biogenic endmember (47). Following previous literature (4), samples with the largest methane concentrations were used to estimate the $\delta^{13}C$ signature of the thermogenic endmember (-28.3‰; red solid line). The initial concentration of thermogenic methane in water before oxidation likely varies temporally and spatially. The [CH_4] concentration of 1000 µg/L (1/[CH_4]=0.001) is chosen to calculate expected Rayleigh fractionation (blue dashed lines). Two scenarios are considered for two values of fractionation factors (α) of 1.013 and 1.025, derived from previous work (48).

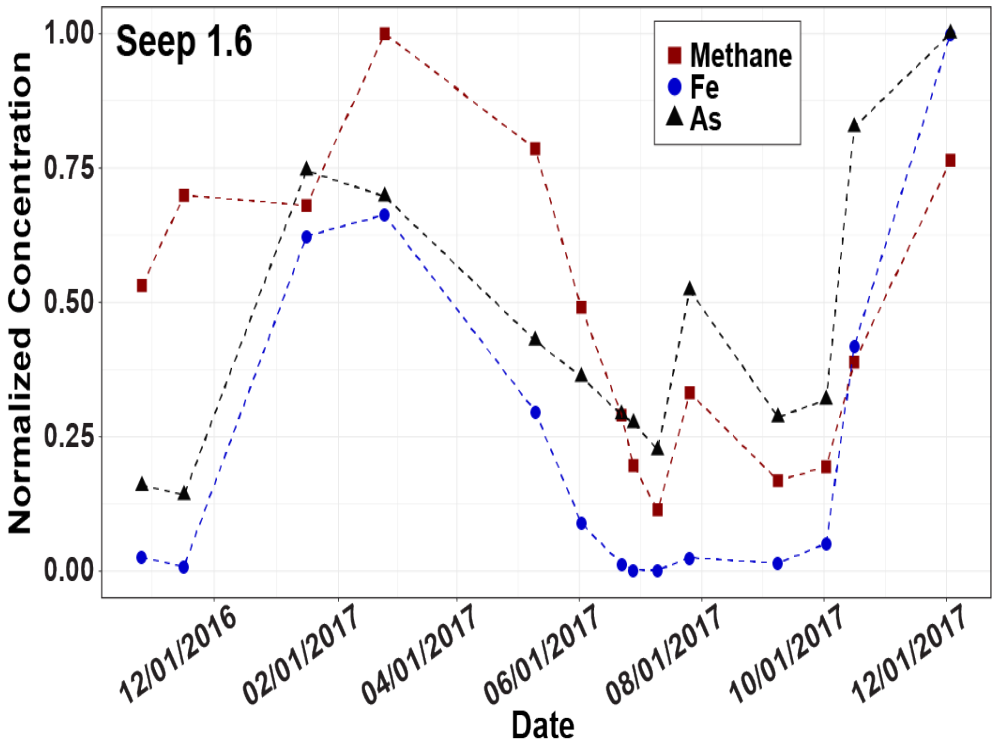

Figure S7. Concentrations of CH_4, Fe, and As in the most methane-rich seep (1.6) plotted versus time. For simplicity, concentrations were normalized by dividing by the maximum values: Fe (17.8 mg/L), As (0.0058 mg/L), CH_4 (8.6 mg/L).

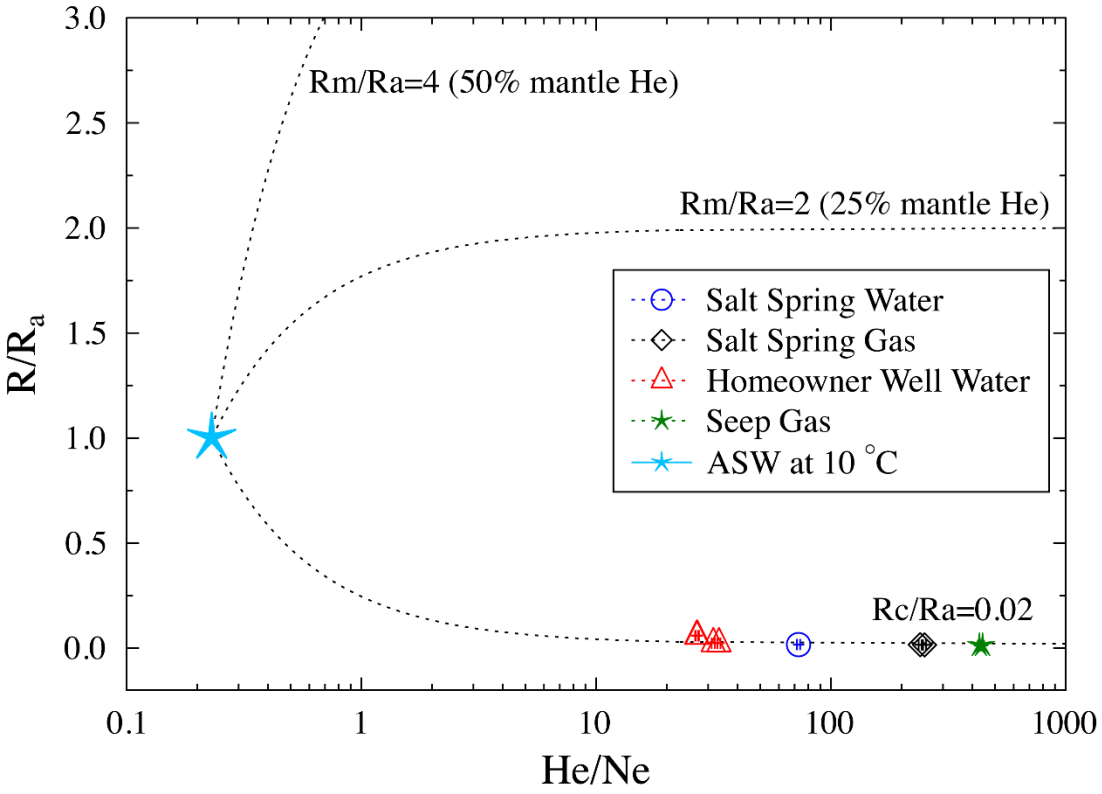

Figure S8. *R/Ra* and He/Ne ratios of all collected noble gas samples including water from the salt spring at Salt Spring State Park, Pennsylvania, and homeowner wells in Sugar Run. Dashed curves represent mixing between noble gases from ASW at 10 °C and radiogenic noble gases (including crustal and mantle sources). Three scenarios with varying contributions of mantle He (i.e., 0%, 25%, and 50% by mass) are indicated. All water and gas samples reported for the Sugar Run area are located on the curve representing mixing between ASW and pure crustal components. This precludes the presence of significant mantle noble gas in these samples.

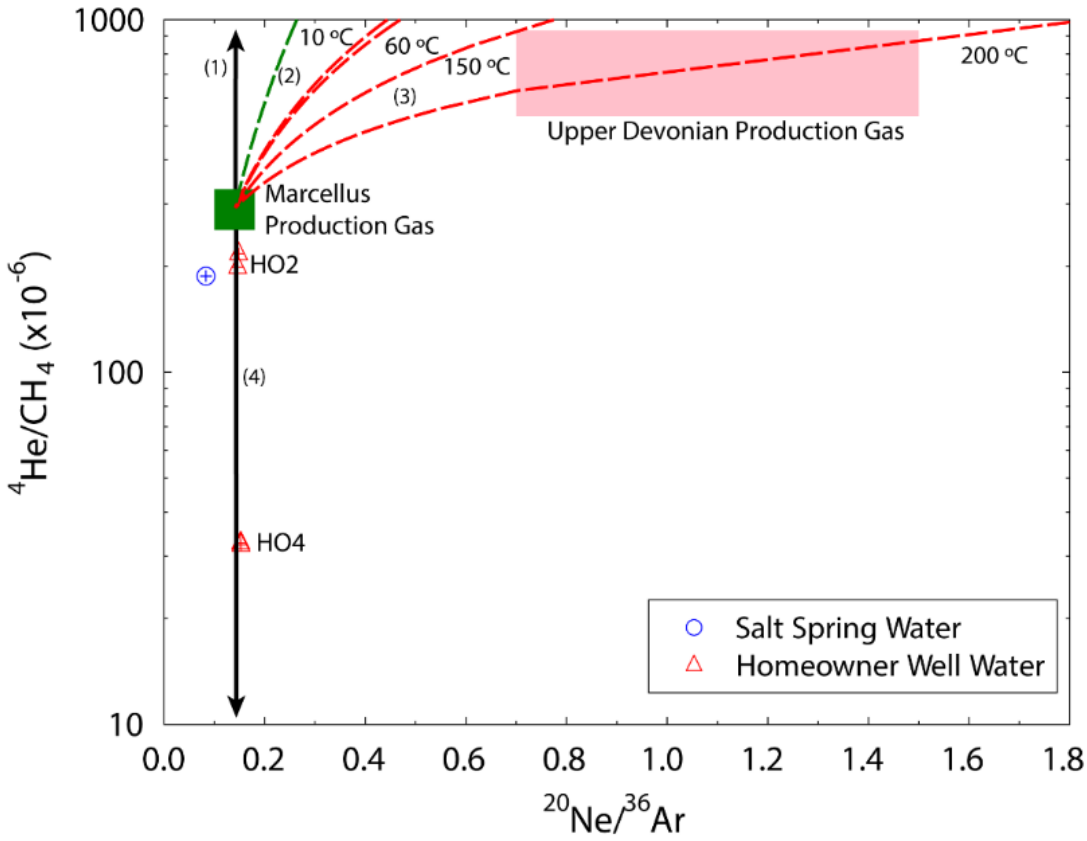

Figure S9. ^{4}He/CH$_4$ and ^{20}Ne/^{36}Ar ratios of homeowner well water samples (red triangles) and salt spring water (blue circle). Short vertical and horizontal lines within sample marks represent corresponding error bars for ^{4}He/CH$_4$ and ^{20}Ne/^{36}Ar, respectively. Predicted values are also plotted for four scenarios: (1) slow upward advection of brine containing dissolved methane (black line with upward arrow); (2) diffusion of gas from depth in aqueous solution (green dashed curve); (3) upward advection of two phases (i.e., free gas phase and brine phase) (i.e., free gas phase and brine phase) from depth (red dashed curves); and (4) fast upward advection of free phase gas with minor mixing of microbial gas in the shallow aquifer (vertical line with downward arrow). Note, we assume that microbial gas contributes methane but not noble gases. In all of these scenarios, we assumed the starting point of noble gas fractionation was the composition of Marcellus Formation production gas (green rectangle). The pink rectangle represents ^{4}He/CH$_4$ and ^{20}Ne/^{36}Ar of natural gas samples from Upper Devonian formations (33). ^{20}Ne/^{36}Ar ratios of homeowner wells HO2 and HO4 are consistent with scenario (4) (fast upward flow of Marcellus gas mixed with biogenic gas), and is not consistent with scenarios (1), (2), nor (3). We hypothesize that relatively quick migration of Marcellus gas along faults in a free gas phase best explains why the homeowner well waters preserve the original ^{20}Ne/^{36}Ar signature.

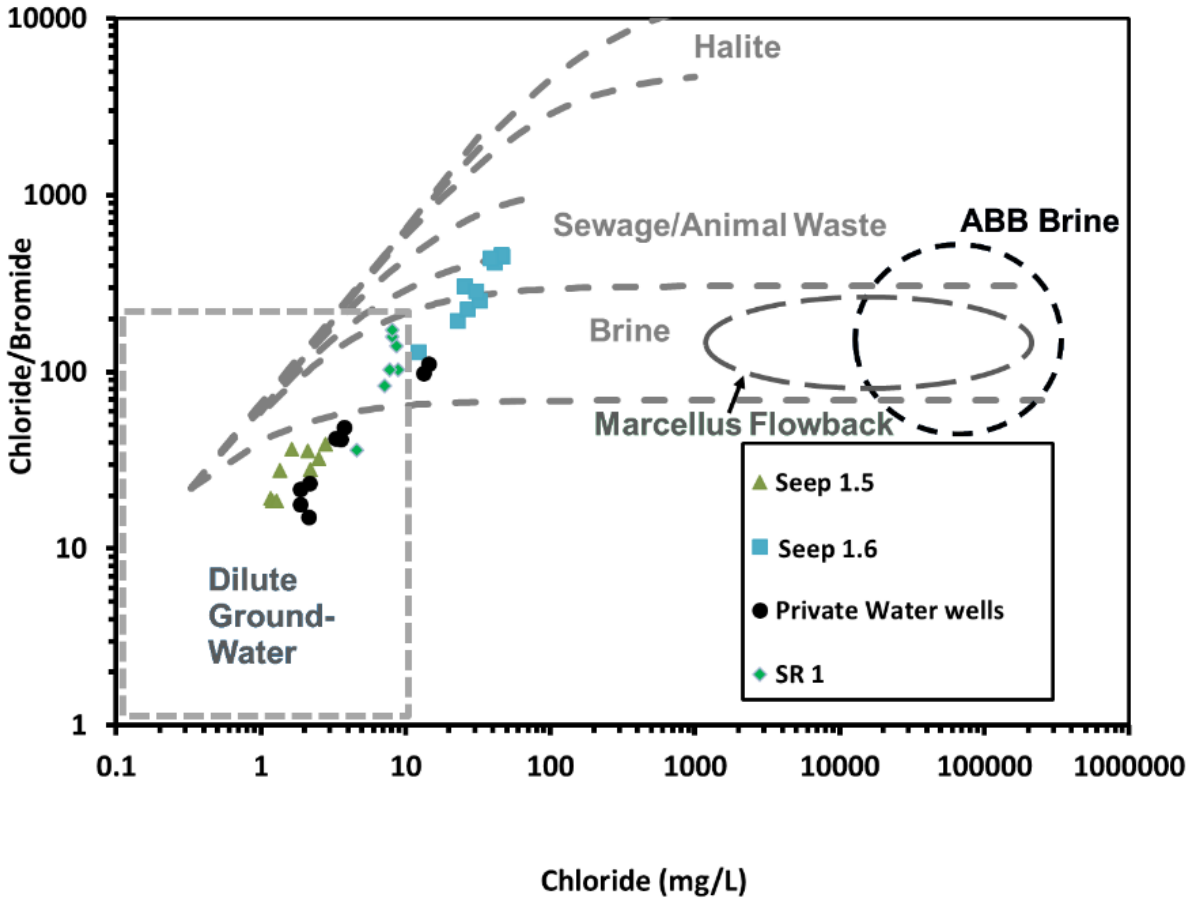

Figure S10. Plot of ratios of Cl/Br concentrations (both as mg/L) versus chloride for samples collected from Seep 1.5, Seep 1.6, stream sample SR 1, and homeowner water wells HO1, HO2, HO3, and HO4. Most waters plot within or very near dilute groundwater except for Seep 1.6. The plot, adapted from previous work, shows generalized regions of different water types (42). The circle labeled "ABB Brine" represents chemistry of directly sampled ABB.

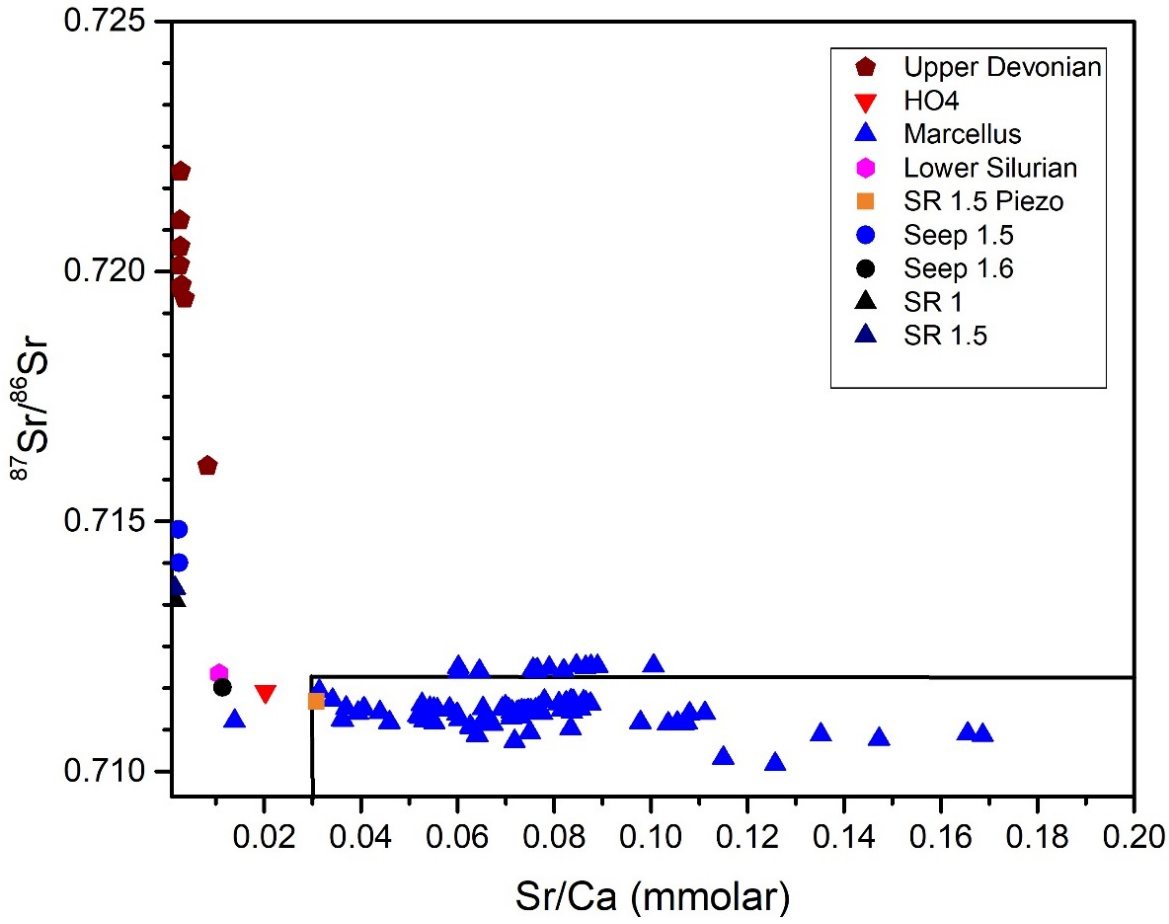

Figure S11. $^{87}Sr/^{86}Sr$ vs Sr/Ca molar ratio in samples taken near Sugar Run (stream samples labelled SR, homeowner well waters labelled HO, groundwater under the stream sampled by piezometers labelled Piezo, and seeps) and brines collected from oil and gas wells (49). The plot shows the possibility that there are two different sources of brine salts that have impacted waters in the Sugar Run valley. The black box encompasses the variation in chemical fingerprint of brines originating from the Marcellus as defined by previous work (43). Samples collected at Seep 1.6, HO4, and SR 1.5 Piezo have the distinctively higher Sr/Ca and lower $^{87}Sr/^{86}Sr$ that are typical of Marcellus brines (43). In contrast, stream sites SR 1 and SR 1.5, and Seep 1.5 show chemical characteristics more consistent with radiogenic upper Devonian formations such as the Bradford Group and Venango Group. Some data values were reproduced here from previous works (4, 11).

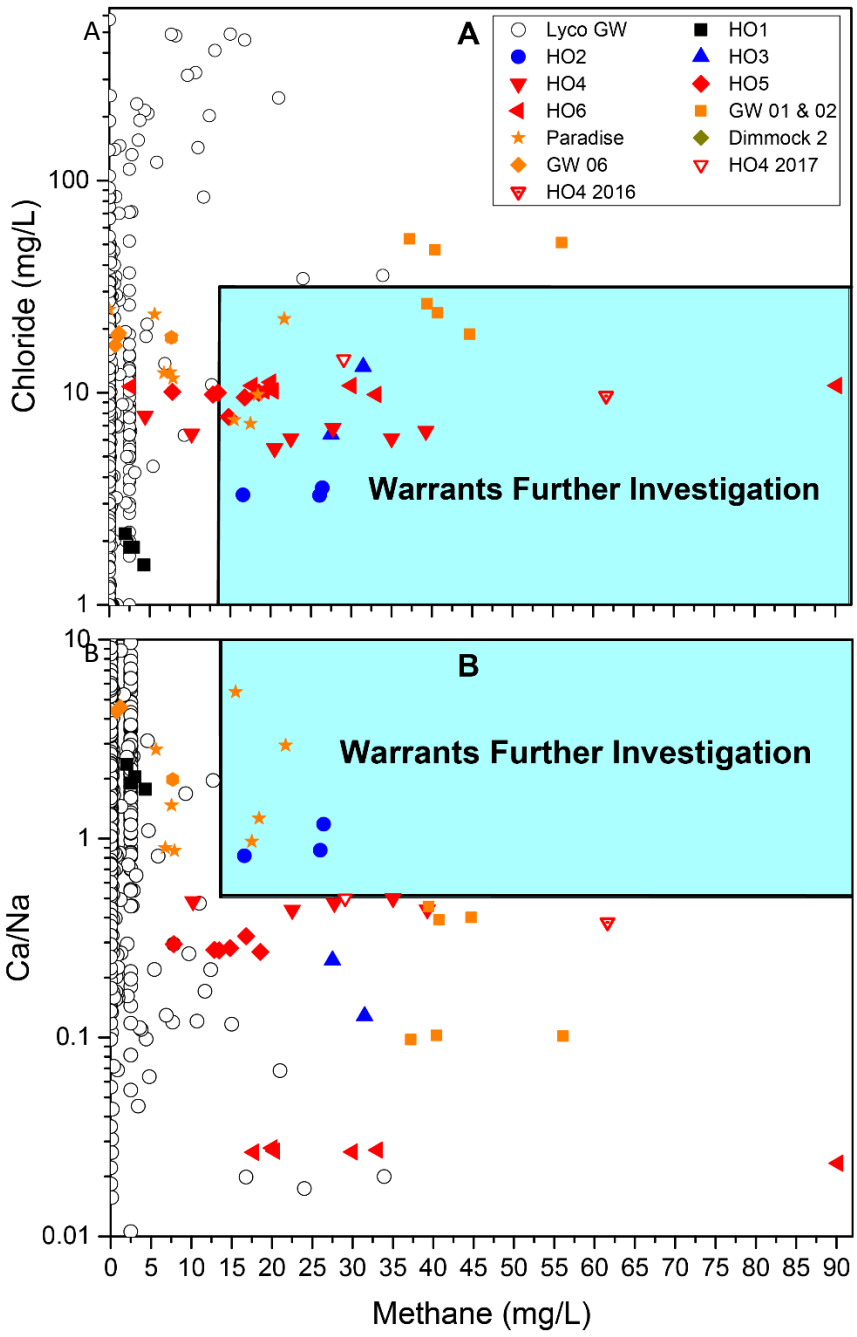

Figure S12. A) Plot of chloride versus methane concentrations in groundwater samples as labelled (see text in SI and main body). Most high methane water in Lycoming county contains high concentrations of chloride. However, waters from almost all locations with presumable contamination, including Sugar Run, contain relatively low concentrations of chloride. B) Ca/Na (mass ratio) versus methane concentrations in groundwater samples as labelled. Most high methane samples contain Ca/Na < 0.52. However, a small subset of presumably contaminated samples contains Ca/Na > 0.52.

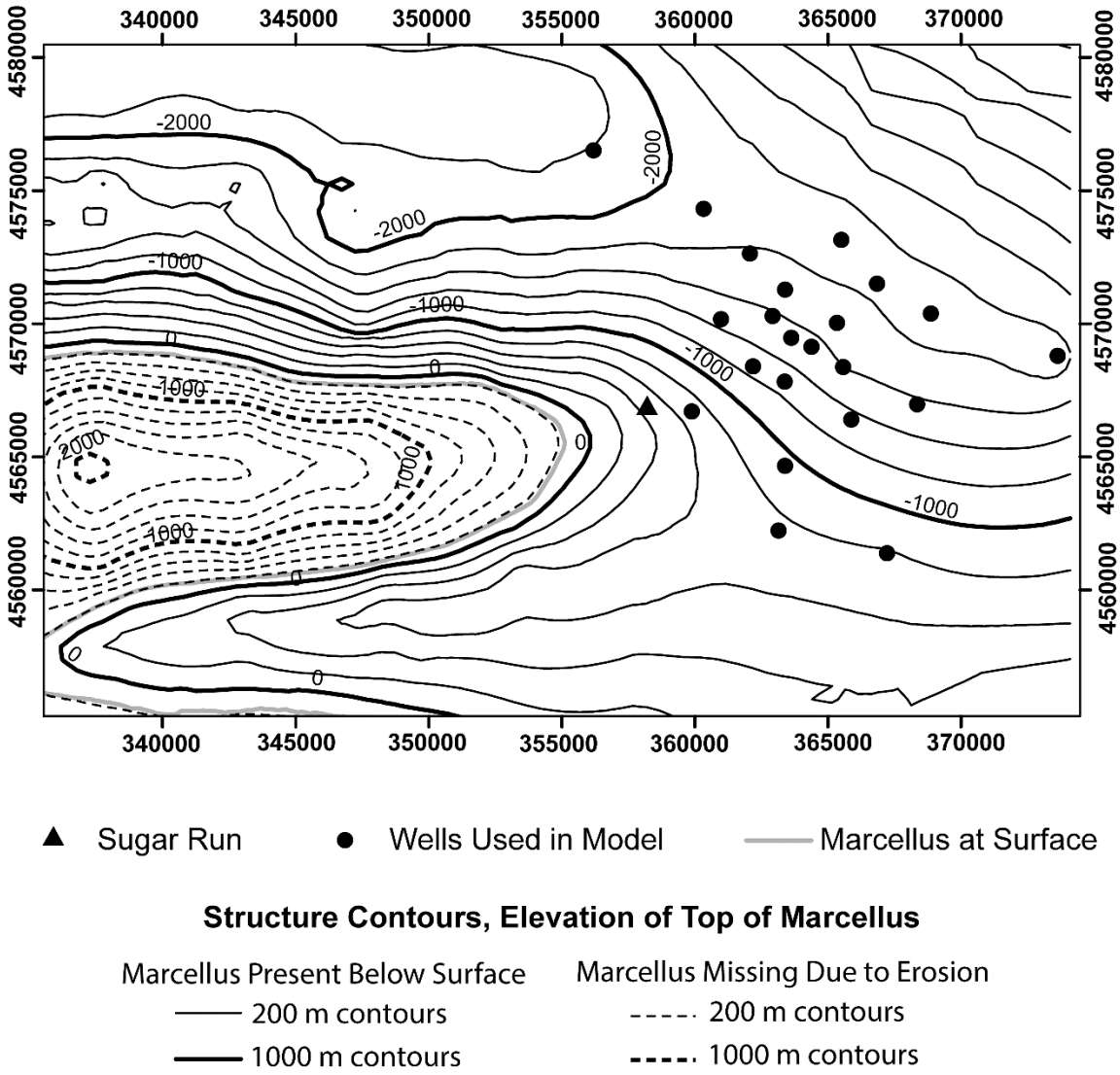

Figure S13. A contour map of depth of the top of the Marcellus Shale (dashed lines document where erosion has removed the shale and negative labels on contours denote depth below sea level in meters). The surface was calculated from cross sections, gas well reports, and topographic data using ordinary kriging. Coordinates are in UTM, Zone 18 North.

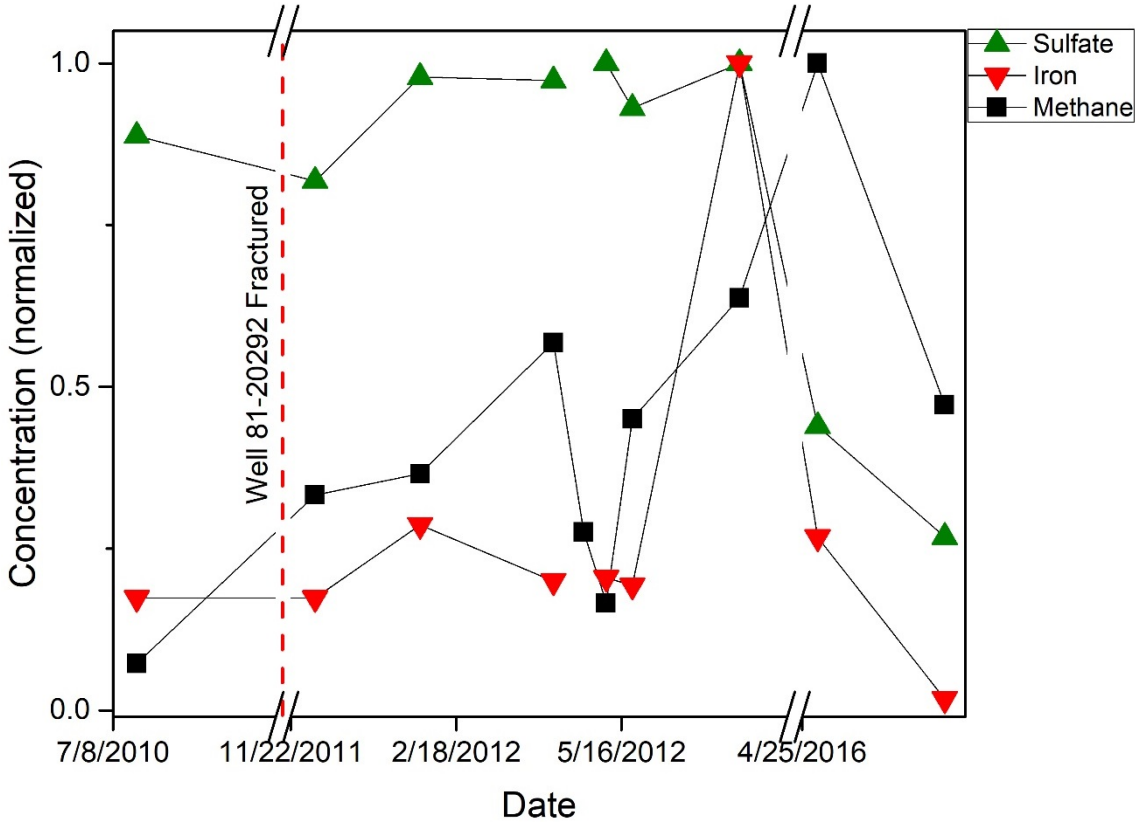

Figure S14. Normalized concentrations of methane, iron, and sulfate versus time for groundwater from homeowner well HO4. Concentrations are normalized to the largest concentration for each analyte: methane = 61.6 mg/L, sulfate = 18.7 mg/L, iron = 0.576 mg/L. Concentrations are only plotted where at least two of the three analytes were available on a given date (Dataset S1).

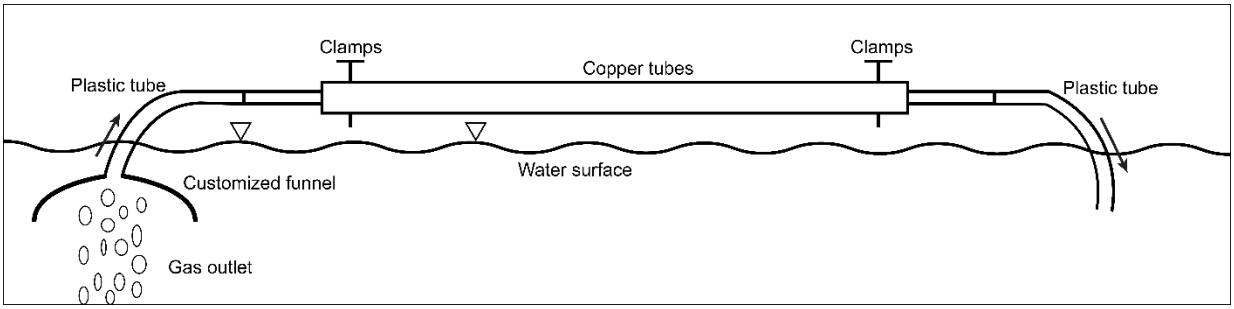

Figure S15. The set-up for the collection of gas samples for noble gas analyses at bubbling seep sites.

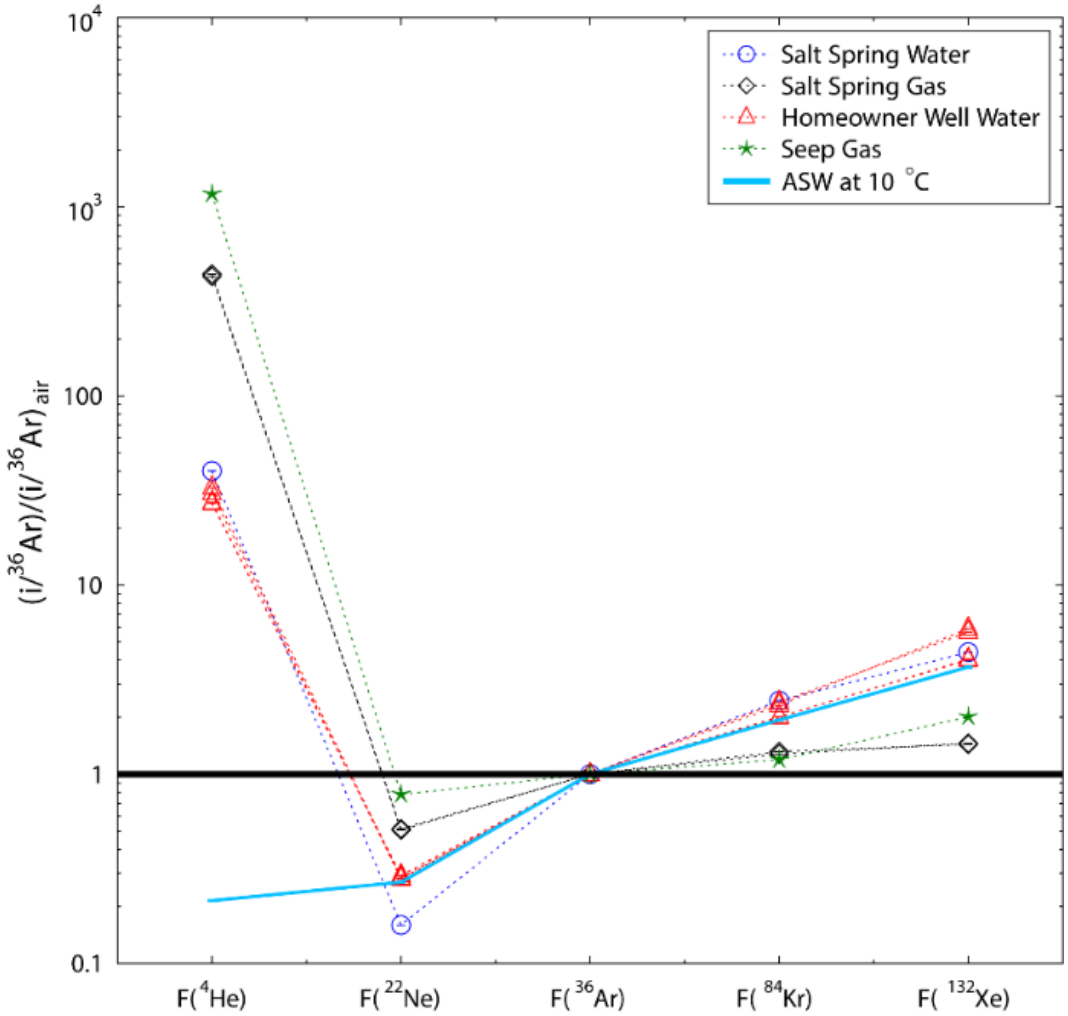

Figure S16. $F(^4He)$, $F(^{22}Ne)$, $F(^{84}Kr)$, and $F(^{132}Xe)$ value of collected water and gas samples. $F(^4He)$, $F(^{22}Ne)$, $F(^{84}Kr)$, and $F(^{132}Xe)$ are measured $^4He/^{36}Ar$, $^{22}Ne/^{36}Ar$, $^{84}Kr/^{36}Ar$, $^{132}Xe/^{36}Ar$ ratios normalized to corresponding air values. *F* values of ASW (air saturated water) at the temperature of 10 °C (light blue line) and air (horizontal black line) are shown for comparison (50).

SI Tables

Table S1. Generalized timeline of events in the study area

Date (m/d/y)	Events: Associated with problematic wells within 5 km of well 081-20292
9/14/2008	Well API # 081-20109 spudded
11/4/2008	Well API # 081-20119 spudded
10/31/2009	Well API # 081-20205 spudded
11/27/2009	Well API # 081-20209 spudded
7/9/2009	Well API # 081-20144 spudded
12/15/2009	Well API # 081-20210 spudded
6/1/2010	Well API # 081-20296 spudded
8/9/2010	Well API # 081-20348 spudded
8/19/2010	Well API # 081-20275 spudded
10/19/2010	Well API # 081-20287 spudded
11/1/2010	19 private water wells located along Green Valley Road in Moreland Township were sampled within 2,500 feet of 081-20292. Methane was detected in four samples.
12/19/2010	Well API # 081-20371 spudded
12/20/2010	Well API # 081-20275 received violation 78.85; DEP observed gas in the 2" vent
12/20/2010	Well API # 081-20348 received two casing-related violations (78.85 & 78.86); DEP observed gas in 2" vent pipe
1/9/2011	Well API # 081-20209 receives two casing-related violations (78.85 & 78.86); DEP observed 18 psi pressure at the 5 ½" x 9 5/8" pipe.
1/9/2011	Well API # 081-20210 received two casing-related violations (78.85 & 78.86); DEP observed 580psi on the 5 1/2" x 9 5/8".
1/9/2011	Well API # 081-20205 received two casing-related violations (78.85 & 78.86); DEP observed 685psi on the 5 1/2" x 9 5/8".
1/9/2011	Well API # 081-20119 received two casing-related violations (78.85 & 78.86); DEP observed 250psi on the 5 1/2" x 9 5/8".
1/9/2011	Well API # 081-20109 received two casing-related violations (78.85 & 78.86); DEP observed 150psi on the 5 1/2" x 9 5/8".
1/26/2011	Well API # 081-20144 received casing-related violations 78.86 & 78.85
2/1/2011	Well API # 081-20241 spudded
2/12/2011	Drilling began for well API # 081-20292

Date (m/d/y)	Events: Associated with problematic wells within 5 km of well 081-20292
3/9/2011	Well API # 081- 20532 spudded
3/17/2011	Drilling completed for well API # 081-20292
3/25/2011	Company received three violations from DEP related to spillage of drilling mud
4/27/2011	Well API # 081-20496 spudded
End 6/2011	Horizontal portion of API # 081-20292 hydraulically fractured
7/6/2011	Well API # 081-20296 received violation 78.86, defective cement; DEP observed gas in the annulus of the 9 5/8" x 5 1/2" casing.
7/10/2011	Well API # 081-20532 received violation 78.86, defective cement; DEP observed gas in the annulus of the 9 5/8" x 5 1/2" casing.
7/10/2011	Well API # 081-20287 received violation 78.86; defective cement; DEP observed gas in the annulus of the 9 5/8" x 5 1/2" casing.
7/10/2011	Well API # 081-20496 received violation 78.86, defective cement; DEP observed gas in the annulus of the 9 5/8 x 5 1/2 casing.
1/9/2012	DEP was given notice of discolored water in water supply near well API # 081-20292
1/18/2012	Water samples were collected from private water supplies for analysis
2/7/2012	DEP inspection found defective cement in annulus of well API # 081-20292 based on shut-in tests
12-Feb	Waters from well API # 081-20292 (three casing strings) and homeowner wells were sampled for isotopic tests
5/14/2012	Gas detected outside surface casing in well API # 081-20292
4/10/2013	Well API # 081-20371 received casing-related violation 78.86; DEP discovered on 4/9/13 that the operator found combustible gas in the 9 5/8" x 5 1/2" annulus on 8/6/12 and that no action had been taken to correct the defect.
9/20/2013	DEP issued a notice of violation (NOV) to well API # 081-20292 for 1) failing to prevent migration of gas or other fluids into ground water (78.81(a)2 and (3)); 2) an unpermitted discharge of gas into surface or groundwaters (violation of section 401 of the Clean Stream Law; 3) defective casing or cementing (violation of section 78.86)
12/13/2013	DEP issued a NOV indicating failure to plug an abandoned well (78.91(a)), referring to well API # 081-20292

Date (m/d/y)	Events: Associated with problematic wells within 5 km of well 081-20292
4/13/2015	Since this date, DEP has investigated potential complaints involving stray gas migration in an area approx. 9,850 feet from well 081-20292 and 5,200 feet from originally affected water supplies noted above. Soil gases measured in a farm field with dead vegetation near Greg's Run contained as much as 100% methane. Combustible gas was also identified in Greg's Run.
5/11/2015	DEP issued order to remediate well API # 081-20292
6/5/2015	Company appealed order to remediate well API # 081-20292
Early 8/2015	DEP and company began making tests and field observations of the water and soil resources
10/22/2015	Company collected logging data from well API # 081-20292
16-Dec	Drilling commenced through a cement plug the in 5.5" production casing in order to prepare well API # 081-20292 for flaring. This attempt to re-enter the lower portion of the casing at approximately 2,540 feet was unsuccessful.
??	Homeowners in the area were offered water treatment systems voluntarily by the company.
3/9/2016	Well API # 081-20241 received violation 78.86; DEP observed 4% methane in 13 3/8" x 95/8" annular vent
6/9/2016	Well API # 081-20371 received violation for 78.86 (pressure still noted in annulus). Well is shut in.
6/14/2016	Waters in wells near Greg's Run (southwest of well API # 081-20292) observed to contain elevated methane and metals.
12/7/2016	Violations at Well API # 081-20296 still outstanding
3/27/2017	Violations at Well API # 081-20241 still outstanding; DEP observed 5% methane on the 13 3/8" x 9 5/8" annulus.
7/31/2018	Eight violations Well API # 081-20292 still outstanding: 78.73(a), 78.81(a)2, 78.81(a)3, 78.86, CSL 301, CSL 307(a), CSL 401, CSL 402(b)

Information in table was summarized and paraphrased from online and published reports (1, 23, 27, 51)

Table S2. Noble gas and methane concentrations (cm^3 STP/gH_2O) of water samples[a].

Sample	Sampling Date	CH_4	He	Ne	Ar	Kr	Xe
HO2-A	7/18/2017	0.0232	4.6091E-06	1.4615E-07	2.6860E-04	7.5827E-08	1.4747E-08
HO2-B	7/18/2017	0.0232	5.0329E-06	1.5090E-07	2.7387E-04	8.0181E-08	1.4405E-08
HO4-A	7/26/2017	0.0686	2.2174E-06	8.2216E-08	1.4475E-04	3.5555E-08	5.4094E-09
HO4-B	7/26/2017	0.0686	2.2490E-06	8.3953E-08	1.4827E-04	3.6238E-08	5.6055E-09
Salt Spring Water	7/17/2017	0.0235	4.4078E-06	6.0571E-08	1.9561E-04	5.8446E-08	8.0483E-09
ASW[b]	-	-	4.4814E-08	1.9457E-07	3.7237E-04	8.7948E-08	1.2779E-08

Sample	^{4}He	^{22}Ne	^{36}Ar	^{84}Kr	^{132}Xe	^{40}Ar*	+/-	^{4}He Age (Ma)
HO2-A	4.6091E-06	1.3480E-08	9.0355E-07	4.3221E-08	3.9653E-09	-	-	0.78
HO2-B	5.0329E-06	1.3906E-08	9.2129E-07	4.5703E-08	3.8735E-09	-	-	0.85
HO4-A	2.2174E-06	7.5831E-09	4.8694E-07	2.0266E-08	1.4546E-09	2.9598E-07	9.2239E-08	0.37
HO4-B	2.2490E-06	7.7427E-09	4.9878E-07	2.0656E-08	1.5073E-09	2.4959E-07	1.4356E-07	0.38
Salt Spring Water	4.4078E-06	5.5972E-09	6.5804E-07	3.3314E-08	2.1642E-09	-	-	0.74
ASW[b]	4.4814E-08	1.7968E-08	1.2527E-06	5.0130E-08	3.4364E-09	-	-	-

[a] Errors of He, Ne, Ar, Kr, and Xe concentrations are 1.5%, 1.3%, 1.3%, 1.5%, and 2.2%, respectively

[b] (50)

Table S3. Noble gas volume fractions (cm^3/cm^3) of gas samples[a]

Sample	Sampling Date	He	Ne	Ar	Kr	Xe
Seep 1.55-1	7/10/2017	2.4923E-04	5.8148E-07	3.8034E-04	5.5354E-08	7.1257E-09
Seep 1.55-2	7/10/2017	2.2308E-04	5.0435E-07	3.3451E-04	4.4825E-08	6.1898E-09
Salt Spring-1	7/17/2017	4.2829E-04	1.7102E-06	1.7291E-03	2.7790E-07	2.3181E-08
Salt Spring-2	7/17/2017	4.2654E-04	1.7786E-06	1.7729E-03	2.7652E-07	2.4059E-08
Air [b]	-	5.2400E-06	1.8180E-05	9.3400E-03	1.1400E-06	8.7000E-08

Sample	^{4}He	^{22}Ne	^{36}Ar	^{84}Kr	^{132}Xe	$^{40}Ar^*$	+/-
Seep 1.55-1	2.4923E-04	5.3395E-08	1.2795E-06	3.1552E-08	1.9161E-09	2.5356E-06	2.4439E-07
Seep 1.55-2	2.2308E-04	4.6267E-08	1.1253E-06	2.5550E-08	1.6644E-09	2.7019E-06	3.257E-07
Salt Spring-1	4.2829E-04	1.5755E-07	5.8167E-06	1.5840E-07	6.2335E-09	-	-
Salt Spring-2	4.2654E-04	1.6381E-07	5.9640E-06	1.5762E-07	6.4695E-09	-	-
Air [b]	5.2400E-06	1.6780E-06	3.1420E-05	6.4980E-07	2.3394E-08	-	-

[a] Errors of He, Ne, Ar, Kr, and Xe concentrations are 1.5%, 1.3%, 1.3%, 1.5%, and 2.2%, respectively

[b] (50)

Table S4. Noble gas isotopic ratios of water and gas samples

Sample	$^{20}Ne/^{22}Ne$	+/-	$^{21}Ne/^{22}Ne$	+/-	$^{38}Ar/^{36}Ar$	+/-	$^{40}Ar/^{36}Ar$	+/-	$^{80}Kr/^{84}Kr$	+/-
Water Samples										
HO2-A	9.8121	0.0018	0.02902	0.00001	0.1878	0.0001	294.9504	0.1935	0.0395	0.0001
HO2-B	9.8204	0.0013	0.02904	0.00001	0.1879	0.0001	295.3313	0.1677	0.0396	0.0001
HO4-A	9.8119	0.0027	0.02901	0.00002	0.1883	0.0001	296.1078	0.1926	0.0395	0.0001
HO4-B	9.8128	0.0026	0.02908	0.00002	0.1880	0.0001	296.0004	0.1748	0.0394	0.0001
Salt Spring Water	9.7935	0.0019	0.02909	0.00003	0.1878	0.0001	295.3836	0.1713	0.0396	0.0001
Gas Samples										
Seep 1.55-1	9.8555	0.0022	0.02928	0.00002	0.1880	0.0001	297.4818	0.1709	0.0393	0.0001
Seep 1.55-2	9.8654	0.0021	0.02924	0.00003	0.1882	0.0001	297.9010	0.1924	0.0394	0.0001
Salt Spring-1	9.8234	0.0016	0.02905	0.00001	0.1878	0.0001	294.9606	0.1635	0.0400	0.0001
Salt Spring-2	9.8262	0.0017	0.02906	0.00002	0.1880	0.0001	295.2091	0.1709	0.0399	0.0001
Air [a]	9.8000		0.02900		0.1880		295.5000		0.0396	

Sample	$^{82}Kr/^{84}Kr$	+/-	$^{83}Kr/^{84}Kr$	+/-	$^{86}Kr/^{84}Kr$	+/-	$^{128}Xe/^{130}Xe$	+/-	$^{129}Xe/^{130}Xe$	+/-
Water Samples										
HO2-A	0.2023	0.0003	0.2015	0.0002	0.3060	0.0004	0.4663	0.0009	6.565	0.013
HO2-B	0.2022	0.0003	0.2012	0.0002	0.3055	0.0004	0.4674	0.0010	6.599	0.012
HO4-A	0.2021	0.0002	0.2013	0.0002	0.3052	0.0003	0.4699	0.0008	6.533	0.012
HO4-B	0.2020	0.0003	0.2011	0.0003	0.3055	0.0004	0.4716	0.0008	6.515	0.013
Salt Spring Water	0.2024	0.0003	0.2013	0.0002	0.3052	0.0004	0.4699	0.0008	6.536	0.012
Gas Samples										
Seep 1.55-1	0.2019	0.0002	0.2014	0.0002	0.3058	0.0004	0.4724	0.0010	6.493	0.012
Seep 1.55-2	0.2018	0.0003	0.2009	0.0002	0.3053	0.0004	0.4708	0.0010	6.497	0.013
Salt Spring-1	0.2021	0.0002	0.2013	0.0002	0.3056	0.0004	0.4693	0.0009	6.533	0.012
Salt Spring-2	0.2021	0.0002	0.2014	0.0002	0.3056	0.0004	0.4702	0.0010	6.519	0.012
Air [a]	0.2022		0.2014		0.3052		0.4715		6.496	

Sample	$^{131}Xe/^{130}Xe$	+/-	$^{132}Xe/^{130}Xe$	+/-	$^{134}Xe/^{130}Xe$	+/-	$^{136}Xe/^{130}Xe$	+/-
Water Samples								
HO2-A	5.251	0.009	6.680	0.007	2.587	0.002	2.198	0.001
HO2-B	5.266	0.009	6.694	0.007	2.593	0.002	2.197	0.002
HO4-A	5.231	0.008	6.646	0.005	2.575	0.001	2.189	0.001
HO4-B	5.226	0.008	6.624	0.006	2.570	0.002	2.183	0.001
Salt Spring Water	5.246	0.008	6.661	0.006	2.585	0.002	2.201	0.002
Gas Samples								
Seep 1.55-1	5.214	0.008	6.593	0.006	2.555	0.002	2.165	0.002
Seep 1.55-2	5.207	0.008	6.601	0.006	2.562	0.002	2.171	0.002
Salt Spring-1	5.227	0.007	6.644	0.005	2.576	0.002	2.190	0.002
Salt Spring-2	5.221	0.007	6.626	0.006	2.566	0.002	2.185	0.002
Air [a]	5.213		6.607		2.563		2.176	

Sample	R/Ra	+/-	$^{4}He/^{40}Ar^{*}$	+/-	$^{4}He/^{20}Ne$	+/-	$^{20}Ne/^{36}Ar$	+/-	$^{4}He/CH_4(x10^{-6})$	+/-
Water Samples										
HO2-A	0.0237	0.0005	-		34.85	0.69	0.146	0.003	198.57	2.98
HO2-B	0.0231	0.0005	-		36.85	0.73	0.148	0.003	216.83	3.25
HO4-A	0.0589	0.0009	7.49	2.34	29.80	0.59	0.153	0.003	32.32	0.48
HO4-B	0.0583	0.0011	9.01	5.18	29.60	0.59	0.152	0.003	32.78	0.49
Salt Spring Water	0.0165	0.0006	-		80.41	1.60	0.083	0.002	187.33	2.81
Gas Samples										
Seep 1.55-1	0.0114	0.0005	98.29	9.59	473.61	9.40	0.411	0.008	-	
Seep 1.55-2	0.0116	0.0004	82.57	10.03	488.74	9.70	0.406	0.007	-	
Salt Spring-1	0.0151	0.0005	-		276.73	5.49	0.266	0.005	-	
Salt Spring-2	0.0160	0.0004	-		265.00	5.26	0.270	0.005	-	
Air [a]	1.0000		-		0.318		0.524	0.010	-	

[a] (50)

Other Supporting Information Files:

Dataset S1: This dataset compiles water chemistry and hydrocarbon data for the Sugar Run area